4. Numerical modelling

4.1 Introduction

The physical processes occurring inside an evaporator vessel are extremely complex when considered in their entirety. However, the physics associated with different parts of the process can be treated separately and some simplifying assumptions applied to build an overall descriptive model. Since this investigation was the first attempt to model an evaporator vessel in its entirety, a number of simplifying assumptions have been applied to build a working model. Each assumption is justified in its use because the effect on the accuracy of the CFD model predictions is less than errors associated with the experimental data.

Numerical modelling of the steady state operation for two different evaporator vessels was carried out in this study. This chapter outlines the equations governing the numerical model. As the physical processes occurring inside an evaporator vessel are extremely complex, the evaporator will be divided into different sections, and simplifications to the model made based on the dominant physical process occurring within each section. Two evaporator vessels being studied are the Proserpine #4 and Farleigh #2 vessels.

Initially the Proserpine #4 and the Farleigh #2 geometries were modelled so that direct comparisons could be made with factory data. Once the accuracy of the model predictions had been confirmed, the model was used to investigate possible improvements in performance. Initially a retro-fit modification to the Farleigh #2 geometry was considered where a majority of the vessel remained unchanged except the juice inlet and outlet and downtakes were included in the calandria. Finally, a totally new design of evaporator geometry was considered. The concept involves a number of smaller calandrias operating in series and is referred to herein as the linear evaporator design. In total, four different evaporator geometries were considered for the modelling phase of this investigation.

4.2 The software package

The software package used to solve the equations for this investigation was CFX version 5.5. CFX contains standard options for most of the physics modelled as part of this investigation but some user defined sub-routines were required. This input file allows for the physics used during this investigation to be reproduced in CFX.

Appendix B contains an example of one of the input files used to model the Proserpine #4 vessel. It includes all of the details used in creating the CFD model used for this investigation. Included with this thesis is a Compact Disk (CD) containing the CFX input files used in this investigation. The inclusion of the input files to this thesis allows for the work to be reproduced by another researcher.

This chapter provides details and explanation of the most significant portions of the CFD model used for this investigation. It includes details of all of the standard features employed and the user defined sub-routines added to the model.

4.3 Model description

Geometrical symmetry, and hence the assumption of flow symmetry, was used to reduce the size of the computational mesh required. This was necessary since the size of the computational mesh was found to be the single largest contributor to the usage of computer memory which was insufficient to model the entire geometry of the vessel. Since there are a large number of symmetric boundaries inside the vessel that would obstruct the flow, it was assumed that asymmetric flows would be discouraged from developing and dominating the flow field.

Details of the four cases considered are as follows:

- The geometry of the Proserpine #4 vessel displays one-quarter symmetry with four juice inlets and one central juice outlet. A single juice inlet and one-quarter of the outlet was modelled with two planes of symmetry;

- The Farleigh #2 vessel displays no actual symmetry since it has a single juice inlet and two different sized juice outlets. However, the difference in outlet size was neglected and it was assumed that the geometry of the vessel displayed one-half symmetry. Half of the inlet and one of the outlets were modelled with one plane of symmetry;

- The geometry of the modifications to the Farleigh #2 vessel displayed one-eighth symmetry with a single circumferential juice inlet and a single central juice outlet. One-eighth of the inlet and the outlet were modelled with two planes of symmetry; and

- The linear evaporator was assumed to be 2-D and was modelled accordingly.

When the geometric symmetry of the vessels was considered it was recognised that geometric symmetry does not guarantee flow symmetry. The errors resulting from artificially induced flow symmetry are minimal in this case, because the boiling action inside the calandria is the dominant force driving the juice flow. It was assumed that the juice flowing up the heating tubes and down the downtakes would quickly dominate any juice flow pattern entering from the inlet. The factory experiments showed large amounts of juice recirculating around inside the vessels and this supports the justification for making this assumption.

In all cases modelled, the steam distribution within the calandria was assumed to be uniform. A uniform heat source was applied everywhere within the calandria section. In the absence of any data in the literature to provide guidelines on steam distribution, the uniform heat source assumption is the normal assumption used for modelling heat exchangers in other industries.

Each evaporator vessel was divided into three sections, one above the calandria, the calandria itself, and one below the calandria with all the juice inlets and outlets. Due to the complexity of the calandria, it is not possible to model all the tubes. A lumped parameter approach is taken whereby the boiling/heat transfer and fluid flow in the pipes are each represented by a single heat flux and pressure drop relationship respectively. The two sections are then linked through boundary conditions that specify the interaction between the sections. In contrast, the first two sections can be modeled directly through solving the Navier-Stokes and heat equations with appropriate turbulence models and physical data correlating juice temperature and brix.

4.4 Governing equations

For this particular case the three conservation equations of interest are the mass, momentum and energy equations defined in terms of the volume fractions (α_l and α_g) as follows:

The continuity equation for the liquid phase:

$$\frac{\partial \rho_l \alpha_l}{\partial t} + \nabla \bullet (\rho_l \alpha_l V_l) = S_C \qquad (4.1)$$

The continuity equation for the vapour phase:

$$\frac{\partial \rho_g \alpha_g}{\partial t} + \nabla \bullet \left(\rho_g \alpha_g V_g\right) = -S_C \qquad (4.2)$$

The momentum equations for the liquid phase:

$$\frac{\partial \alpha_l \rho_l V_l}{\partial t} + \nabla \bullet \left(\alpha_l \rho_l V_l V_l\right) = -\alpha_l \nabla p + \alpha_l \mu_l \nabla^2 V_l + \alpha_l \rho_l g + S_M \qquad (4.3)$$

The momentum equations for the vapour phase:

$$\frac{\partial \alpha_g \rho_g V_g}{\partial t} + \nabla \bullet \left(\alpha_g \rho_g V_g V_g\right) = -\alpha_g \nabla p + \alpha_g \mu_g \nabla^2 V_g + \alpha_g \rho_g g - S_M \qquad (4.4)$$

The energy equation for the liquid phase:

$$\frac{\partial \alpha_l \rho_l h_l}{\partial t} = -\left(\nabla \bullet \alpha_l \rho_l V_l h_l\right) - \left(\nabla \bullet \alpha_l q_l\right) + S_E \qquad (4.5)$$

The energy equation for the vapour phase:

$$\frac{\partial \alpha_g \rho_g h_g}{\partial t} = -\left(\nabla \bullet \alpha_g \rho_g V_g h_g\right) - \left(\nabla \bullet \alpha_g q_g\right) - S_E \qquad (4.6)$$

The equation for the transport of sugar:

$$\frac{\partial B}{\partial t} + \nabla \bullet (VB) = \left((\rho k_l) \nabla \bullet \left(\frac{B}{\rho} \right) \right) \qquad (4.7)$$

The energy equation as shown in equations (4.5) and (4.6) has neglected the rate of work done by pressure forces and viscous forces. As velocities gradients are small except at the inlet or outlet regions and the viscosity is low for the sugar solutions, the contribution is small relative to the enthalpy of the fluid, and as such can be neglected. Work done by the pressure force is converted into kinetic energy with very little dissipation and hence does not contribute significantly to increasing the heat balance of the fluid. The rate of work done by gravitational forces is accounted through the additional source term.

The region above and below the calandria is assumed to be liquid only and the liquid phase equations are solved in these regions.

For the calandria, rather than solving the multi-phase equations detailed above, a lumped parameter model simplified the equations through the pressure term. The pressure drop inside the calandria section was separated into the three directional components, (see section 4.8.2) such that $S_{Mx} = \frac{\partial p}{\partial x}$ and $S_{Mz} = \frac{\partial p}{\partial z}$ as detailed in equations (4.8) and $S_{My} = \frac{\partial p}{\partial y}$ as detailed in equation (4.9). This is a reasonable assumption since the vertical orientation of the heating tubes inside the actual vessel will prevent any fluid flow in the horizontal plane and the resulting fluid flow in the vertical direction is a simple flow through a smooth pipe. Details of terms used in these equations are described in more detail in section 4.7.2.

4.5 Fluid properties

Fluid properties of the liquid and gas phases are required for the numerical solution of the model. The important properties are specific heat capacity, density, viscosity, boiling point elevation temperature and thermal conductivity. These properties have been correlated as functions of the fluid temperature and sugar concentration, and summarized in Appendix C. The properties of the gas phase have been assumed to be constant as the boiling takes place at a constant temperature. The gas phase properties are obtained from steam tables based on the headspace pressure measured in the vessel.

4.5.1 Fluid temperature

The software package used assumes that the fluid is compressible if it is a function of temperature and automatically invokes the total energy model for solving the energy balance. The total energy model is computationally expensive and not required, as the density does not change significantly with temperature. To enable the program to continue to use the thermal energy model where incompressible flow is assumed, a constant temperature was substituted into the expression for liquid density. This constant temperature was set to be equal to the juice temperature at the inlet to the vessel. As shown in Chapter 5, the change in temperature in the vessel is quite small and this constraint should not affect the calculations and the conclusions significantly.

4.5.2 Sugar concentration

The transport equation for the sugar concentration in the evaporator requires the diffusion coefficient of sugar in water. The kinematic viscosity of sugar varies from $0.9\text{x}10^{-6}$ $m^2{\cdot}s^{-1}$ at 0 wt% sugar to $1.2\text{x}10^{-6}$ $m^2{\cdot}s^{-1}$ at 22 wt% sugar to $3.7\text{x}10^{-6}$ $m^2{\cdot}s^{-1}$ at 40 wt% sugar. The Prandtl number (ratio of thermal diffusivity to kinematic viscosity) for boiling water is approximately 1.7 at atmospheric pressure and increases with decreasing pressure. For low sugar concentrations, the increase in liquid viscosity with increasing sugar concentration compensates against the increase in Prandtl number due to decreasing pressure. The maximum sugar concentration at the outlet is 65% where the Prandtl number is approximately 3.5 times the corresponding Prandtl number for water. Based on the properties of the sugar solution, the thermal diffusivity of the solution is taken to be approximately that of the kinematic viscosity as the data for kinematic viscosity is available but not that of thermal diffusivity.

4.6 Boundary conditions

The boundary conditions are $U_I = 0$, $\frac{dU}{dr} = 0$ for all the solid boundaries. The inlet boundary conditions were based on the experimental values obtained from the factory vessels (see Table 3.11 and Table 3.12). Although the juice flowing into the inlet of the vessel has a small amount (approximately 5%) of vapour mixed in with the liquid, this amount is small and has been neglected. Table 4.1 and Table 4.2 summarises the boundary conditions applied to the inlet for the four cases modelled on the Proserpine #4 vessel and the six cases modelled on the Farleigh #2 vessel.

Table 4.1 Summary of the inlet boundary conditions for the CFD model of the Proserpine #4 vessel

Test no.	**1**	**2**	**3**	**4**
Juice mass flow rate at inlet ($m^3 \cdot h^{-1}$)	258.2	267.7	272.1	273.1
Juice temperature at inlet (°C)	87.8	88.9	81.3	81.3
Juice brix at inlet (%-wt)	35.6	36.3	37.7	38.1

Table 4.2 Summary of the inlet boundary conditions for the CFD model of the Farleigh #2 vessel

Test no.	**1**	**2**	**3**	**4**	**5**	**6**
Juice flow rate at inlet ($m^3 \cdot h^{-1}$)	365.3	315.3	262.8	277.7	344.9	341.0
Juice temperature at inlet (°C)	100.8	100.9	100.4	99.8	95.2	101.0
Juice brix at inlet (%-wt)	22.5	21.7	23.9	22.7	22.1	22.4

The outlet boundary condition was $P = 0$ Pa. Applying a zero pressure at the outlet allows the pressure at the inlet and everywhere else in the fluid domain to be calculated relative to the outlet. This process was adopted to avoid numerical problems with large absolute values of pressure and because the pressure drop from inlet to outlet is the value of interest and is small in magnitude. If required, the absolute magnitude of the pressure at inlet and outlet can be calculated by adding the absolute pressure measured in the headspace of the vessel.

The free surface of the fluid above the calandria was modelled as a rigid lid to the fluid domain. This surface was assigned a free slip boundary condition to allow lateral movement of the fluid without pressure drop. The height of the free surface above the top of the calandria was set according to the measurements of free surface height taken as part of the factory experiments.

4.7 Geometrical considerations

Geometrical details incorporated into the Proserpine #4 and Farleigh #2 models are detailed as follows:

- The Proserpine #4 vessel was modelled with one-quarter symmetry and symmetry planes at the boundary of the cut. The vessel includes a deflector plate placed immediately above the vertical inlet pipe and this was modeled as a rigid thin surface. The no-slip wall boundary conditions for velocity were applied to this surface. A single juice inlet and one quarter of the outlet was modeled with two planes of symmetry.

- The Farleigh #2 vessel displays one-half symmetry with two juice outlets and a single manifold type juice inlet. A single juice outlet and half of the juice inlet manifold were modelled with one plane of symmetry the boundary of the cut.

4.7.1 The calandria

The extremely large number of heating tubes in the calandria section made it impractical to model each tube individually. In order to simplify the modeling, the tubes were lumped into a single pressure drop. The physical orientation of the vertical heating tubes restricts the fluid flow to the vertical direction only. The calandria region operates to transfer heat from the steam side to the juice and effects boiling. The generation of vapour results in a two-phase mixture that separates further up the tube. The boiling provides a buoyancy force and this is modeled as a series of momentum sources. The flow in the tube is assumed to be transitional and a correlation based on the Colebrook equation was used. This new correlation fitted the Colebrook equation in the region of Re to 10000 (the Re of the problem varied between 100 and 7000) and was easier to estimate the friction factor than the Colebrook equation itself (Figure 4.1).

The Colebrook equation was used for this investigation because of its simplicity and it can be easily incorporated into the lumped parameter model. A two-phase equation such as the Lockhart-Martinelli is more accurate but requires inputs that are not specifically calculated by the lumped parameter model. In order to set up a differential equation for the vapour and liquid fractions, the individual heating tubes would have to be modelled. This was not possible during this investigation.

4.7.2 Flow constraint

The pressure drop is constrained to ensure that the fluid flow is essentially in the vertical direction, in accordance with the flow in the tubes. The larger diameter downtakes were modelled separately, but the heating tubes were modeled as a single entity due to the large number of small diameter tubes. A series of momentum sources, through a pressure drop relationship, were used to describe the flow inside the heating tubes. The basis for this approach is that the tubes direct the liquid flow upwards inside the heating tubes and down into the downtakes. The pressure losses associated with the liquid flow and vapour generation is essentially in the vertical direction as the flow is constrained. To constrain the flow, a pressure drop relationship was used to limit the horizontal flows. A pressure term in this case merely changes the flow and does not add to the energy balance.

The default geometry of the vessels defined by CFX oriented that the y-axis as vertical. In this work the pressure drop in the two horizontal directions (x and z) were modelled as a momentum source, according to:

$$\frac{\partial p}{\partial x} = -50.0\rho_l \sqrt{\left(u^2 + v^2 + w^2\right)}u$$

$$\frac{\partial p}{\partial z} = -50.0\rho_l \sqrt{\left(u^2 + v^2 + w^2\right)}w \qquad \textbf{(4.8)}$$

The momentum sources detailed in equation (4.8) were defined in a form where the magnitude of the momentum source would always act in the opposite direction to the fluid flow. The magnitude of the momentum source was also allowed to change according to the magnitude of the velocity vector. For example, a large momentum source would be applied to a node with a large velocity component in the horizontal plane and the magnitude of this momentum source would reduce as the flow approached the vertical orientation. This was found to have a significant influence on the time required for convergence. Simply applying a large momentum source in the horizontal plane all of the time required significantly larger simulation times.

The pressure drop in the vertical direction (y), assuming the fluid flow to be laminar and single phase, was approximated by:

$$\frac{\partial p}{\partial y} = -f\left(\frac{|v|^2 \rho_m}{A_o 2d}\right) \qquad \mathbf{(4.9)}$$

The A_o term is used in equation (4.9) to account for the tube area relative to the calandria section area.

The friction factor (f) as applied in equation (4.9) is a modified version of the Colebrook equation. Since the flow in the calandria section of this vessel is predominantly in the laminar and transitional flow regions, an explicit form of the friction factor equation was used to avoid the iterative nature of the Colebrook. Figure 4.1 shows a plot of the standard friction factor equations for laminar and turbulent flow and the modified equation applied in this case. The final form of the equation used is:

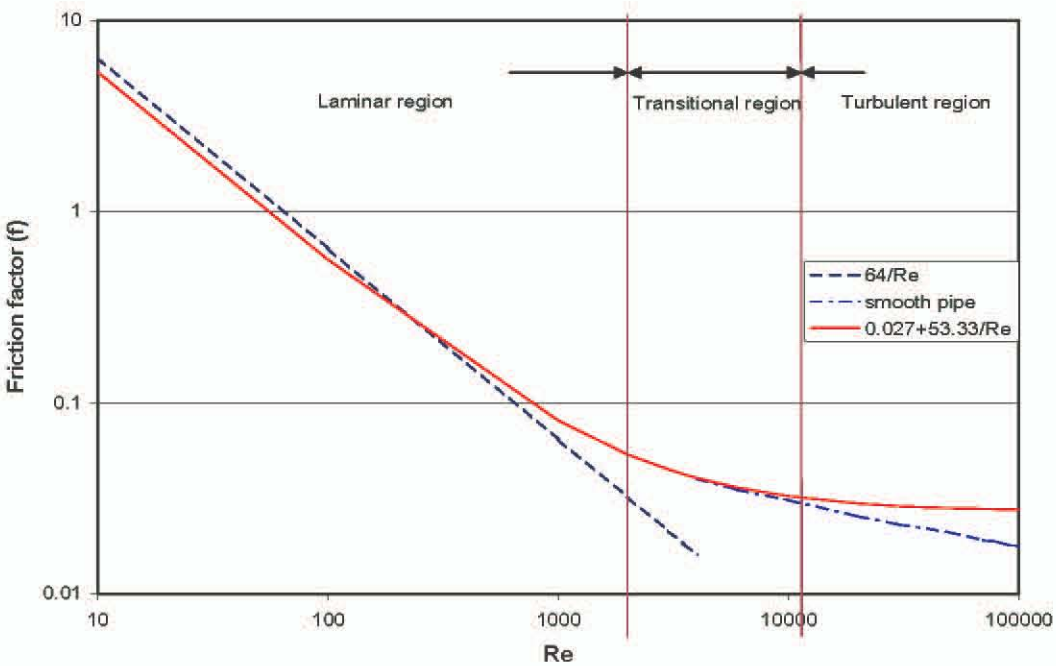

Figure 4.1 Plot of friction factor versus Reynolds Number

$$f = 0.027 + \frac{53.33}{\mathrm{Re}} \quad (4.10)$$

Figure 4.1 shows that the modified equation slightly under-estimates the friction factor at very low Reynolds Numbers and slightly over-estimates the friction factor at higher Reynolds Numbers in the turbulent region but allows for a smooth transition through the transitional region that the standard equations do not. The largest Reynolds Number experienced in the calandria region is approximately 7000, for which the friction factor from equation (4.10) agrees well with the Colebrook equation.

4.7.3 The gaseous phase

The total two phase flow in the boiling region is the sum of the component flows such that $W = W_g + W_l$. The volumetric rate of flow, represented by the symbol Y, is given as a total sum of the volumes $Y = Y_g + Y_l$. Since $Y = \frac{W}{\rho}$, substitute to get $\frac{W}{\rho} = \frac{W_l}{\rho} + \frac{W_g}{\rho}$ and take $\frac{W_g}{W} = X$ and $\frac{W_l}{W} = (1 - X)$. The average density then becomes:

$$\frac{1}{\rho_m} = \frac{X}{\rho_g} + \frac{(1 - X)}{\rho_l} \quad (4.11)$$

where X is the mass fraction of vapour present.

Similarly, the viscosities are assumed to be linearly summable. Although this assumption is an analogy, it provides a reasonable assumption of the average viscosity. The average viscosity then becomes:

$$\frac{1}{\mu_m} = \frac{X}{\mu_g} + \frac{(1 - X)}{\mu_l} \quad (4.12)$$

The calculation of Reynolds Number is performed using the averaged fluid properties such that:

$$\mathrm{Re} = \frac{\rho_m V d}{A_o \mu_m} \quad (4.13)$$

In the calculation of the flow inside the calandria, the liquid and gas phases were modelled as a single phase to simplify the calculations. In so doing, the slip velocity between the liquid and gas phases were assumed to be small. Terminal velocities of air bubbles in pure water varies from 0.2 to 0.4 m/s depending on the bubble size (0.001 to 0.04 m diameter), and hence the terminal Reynolds number, as discussed by Clift *et al.* (1978). With the addition of impurities, it has been found that the terminal velocities are reduced to around 0.2 m/s for the same bubble size range. The effect of relative viscosity has been discussed by Clift *et al.* (1978) and is found to be small but the results have not been obtained for liquids of high viscosities. In the case of slug flow, the terminal velocity has been found to reduce inverse proportionally to the kinematic viscosity; hence a doubling of the kinematic viscosity will reduce the terminal velocity by half. The case in the calandria will be somewhere in between, with the walls of the calandria having a small effect on the bubbles, depending on size. A finite wall also reduces terminal velocity, the extent dependent on the bubble to heating tube diameter ratio. As the space above the calandria shows some degree of foaming, it is expected that the bubbles are not large.

The impurities and viscosity of the juice will act to prevent coalescence of the bubbles formed due to boiling. As such the slip velocities between the liquid and gas phases will not be large, in this case, it should be less than 0.2 m/s, possibly much lower. However, there is a dearth of information regarding the bubble terminal rise velocity for juice and it is recommended that future work should include a study of the bubble terminal rise velocity. The results from the simulations show that the slip velocity of the liquid and gas phases, if included, will not dominate the flow. To a first order, the deletion of the slip velocity should not severely affect the results of the simulation, however, a more accurate model should include the effect of slip velocity.

The assumption of zero slip velocity allowed the calculation of the average fluid properties in each controlled volume, since the liquid and gas were assumed to be flowing at the same velocity. As a result of this calculation the density of the fluid inside the calandria was reduced. The lighter fluid inside the calandria behaved more like the actual fluid where the bubbles would rise up through the liquid inside the heating tubes.

For those cases where the calandria of the vessel was fitted with downtakes, these geometries were modelled specifically. It was assumed that no juice heating occurred inside the downtakes and therefore no vapour was produced. The walls of the downtakes were included as thin surfaces with free slip boundary conditions. Only the momentum source acting in the vertical direction, see equation (4.9), was applied to the fluid flowing inside the downtake. The fluid was allowed to flow laterally inside the down-take since this is what occurs in reality.

The juice flowing into the vessel through the inlet was modelled as liquid phase only. The quantity of vapour resulting from the juice flashing before entering the vessel was neglected. The quantity of flashing was calculated to be approximately 5% of the total mass flow rate of juice at the inlet and contains approximately 13% of the heat which is transferred through the calandria. All of the juice inlet systems considered in this investigation are fitted with distribution devices which spread the incoming liquid and vapour immediately before the flow enters the bulk of the liquid. These devices will spread the juice in all directions and reduce the effect that the vapour has on the flow field in the remainder of the vessel. Modelling of the vapour phase in the incoming juice will add significant complexity to the CFD model and will require significantly more computing resources than are currently available.

4.8 Heat flow inside the calandria

The total thermal energy (Q), released by the condensing steam, neglecting thermal losses, was assumed to go into the latent heat of evaporation, producing vapour and sensible heating of the remaining liquid, due to the effect of boiling point elevation.

$$Q = Q_e + Q_s \tag{4.14}$$

where:

$$Q_e = \dot{m}_e h_{fg} \tag{4.15}$$

$$Q_s = \dot{m}_{in} Cp_l (T_s - T) \tag{4.16}$$

The two components of the heat flow (Q_e & Q_s) were applied as a boundary condition and set as two separate source terms in the energy and the continuity equations. The source term in equation (4.5) was set such that $S_E = Q_s$. The amount of heat that flows into the vapour during the evaporation process was accounted for in the mass source term in equation (4.1) such that $S_C = \frac{Q_e}{h_{fg}}$. To prevent evaporation from occurring before the juice reached it boiling temperature, the source term was linked to the temperature of the fluid such that:

$$S_C = \begin{cases} 0, T < T_s + T_e \\ \dot{m}_e, T \geq T_s + T_e \end{cases} \tag{4.17}$$

Initially the total heat flow (Q) was set to be equal to the experimentally measured value for each test condition. This was required for comparison purposes since the heat flow determined the evaporation rate and therefore the sugar concentration. So it was necessary when comparing factory measurements with predictions to apply the same evaporation rate.

After the initial model comparisons were completed, all of the test conditions were re-modelled such that the total heat flow (Q) was calculated. The total heat flow was calculated according to the following equation, which was developed by Rohsenow (1952) and is detailed in Incropera and DeWitt (1996):

$$\frac{Q}{A} = \mu_l h_{fg} \left[\frac{g(\rho_l - \rho_g)}{\sigma_l} \right]^{1/2} \left(\frac{Ja}{C_{sf} \Pr^n} \right)^3 \tag{4.18}$$

The values of C_{sf} and n as applied in equation (4.18) were set to typical values for water and stainless steel as displayed in a table taken from Incropera and DeWitt (1996). The magnitude of these values were $C_{sf} = 0.013$ and $n = 1.0$ accordingly.

Equation (4.18) was developed predominantly for water and considered a number of different surface types, of which included stainless steel as in this case. The form of the equation is considered suitable for application in this case because it takes into account the effect of varying fluid properties and varying surface-fluid interactions on heat transfer. The fluid properties of sugar solutions at lower concentrations are very similar to water.

A similar study by Hong *et al.* (2004), published after the completion of this investigation, supports the justification for the use of equation (4.18). Hong *et al.* (2004) conducted a comprehensive experimental investigation into the effect of varying fluid properties on heat transfer and the data correlated well with an equation in the same form as equation (4.18). However, the influence of fluid properties was accounted for by modifying the value for C_{sf} as follows:

$$C_{sf} = \frac{0.04}{1 + (B/14.75)^{2.02}} \tag{4.19}$$

Where B is the concentration of sugar (%(w/w)), otherwise referred to as brix for the purposes of this investigation. Equation (4.19) was obtained experimentally using a linear regression.

Hong *et al.* (2004) reports errors of $\pm 10\%$ from the modified form of the equation and this is significantly more accurate than many other heat transfer equations. The success of Hong *et al.* (2004) suggests that the current equation may have the potential to be modified to take into account more of the physics and produce accurate heat transfer predictions. However, further investigation is required in order for this to be demonstrated.

The effect of scale growth on the surfaces of the heating tubes has been neglected for this investigation. Equation (4.18) has the potential to take into account the effect of scale growth by changing the values of C_{sf} and n. However, successful validation the CFD model requires more accurate experimental data than is currently available.

4.9 Fluid flow above the calandria

The fluid flow above the calandria was assumed to be all liquid phase with small buoyancy forces arising from the liquid density variation with sugar concentration. This is similar to the fluid flow below the calandria. However, when applied to the region above the calandria this assumption is far from reality. The fluid above the calandria will have significant variation in liquid mass fraction. The fluid emerging from the top of the calandria will have a liquid mass fraction less than 1, caused by the evaporation process inside the calandria. At the free surface of the fluid the vapour will disengage from the liquid phase and so leave the behind the liquid phase with a liquid mass fraction equal to 1. The variation of fluid quality with vertical height is likely to be highly non-linear.

There is no information in the literature to describe this variation and the determination of such was considered to be outside the scope of the factory experiments conducted as part of this investigation. For these reasons the fluid quality in the region was set to be equal to 1 and the presence of the vapour phase was therefore neglected. The justification for making this assumption is that a fluid quality equal to 1 will produce the largest possible buoyancy forces trying to force any of the heavy juice above the calandria to flow back down the heating tubes or the small down-takes. This has been observed to occur in reality and although the absolute magnitude of the forces involved may be calculated incorrectly, the basis for the fluid behaviour remains correct.

4.10 Turbulence modelling

The $k-\varepsilon$ model was used in this simulation to model turbulence. The two equations for the turbulence kinetic energy (k) and the turbulence dissipation rate (ε)are as follows:

$$\frac{\partial(\rho k)}{\partial t}+\nabla\bullet(\rho Vk)=\nabla\bullet\left[\left(\mu+\frac{\mu_t}{\sigma_k}\right)\nabla k\right]+P_k-\rho\varepsilon \qquad (4.20)$$

$$\frac{\partial(\rho\varepsilon)}{\partial t}+\nabla\bullet(\rho V\varepsilon)=\nabla\bullet\left[\left(\mu+\frac{\mu_t}{\sigma_\varepsilon}\right)\nabla\varepsilon\right]+\frac{\varepsilon}{k}\left(C_{\varepsilon1}P_k-C_{\varepsilon2}\rho\varepsilon\right) \qquad (4.21)$$

where P_k is the turbulence production due to viscous and buoyancy forces, which is calculated as follows:

$$P_k=\mu_t\nabla V\bullet\left(\nabla V+\nabla V^T\right)-\tfrac{2}{3}\nabla\bullet V\left(3\mu_t\nabla\bullet V+\rho k\right)+P_{kb} \qquad (4.22)$$

The values for the constants are $C_{\varepsilon1}$ = 1.44, $C_{\varepsilon2}$ = 1.92, C_μ = 0.09, $\sigma_k=1.0$ and $\sigma_\varepsilon=1.3$. The use of a turbulence model for modelling the turbulence present in a flow is required to provide closure to the Reynolds averaged N-S equations. The $k-\varepsilon$ turbulence model used in this numerical work is a second-order model wherein the stress-equations are included. A turbulent kinetic energy equation and a dissipation rate equation are solved to obtain the turbulent viscosity. The $k-\varepsilon$ turbulence model here is a low Reynolds number form here following that of Jones and Launder (1972) where the model constants are standard and have not been adjusted. Adjustment of the constant is not recommended except when good quality experimental data is available for comparison and evaluation. A law of the wall is used to treat the inner region.

The flow is not highly complex, except in the tubes in the calandria. Elsewhere, the flow generally follows a smooth path from inlet to outlet, possibly with substantial bypassing, to avoid the calandria region. As such the $k-\varepsilon$ model should provide a reasonable estimation of the influence of turbulent dissipation, although it is generally more dissipative. The more complex turbulence models are able to better predict turbulence but are less stable.

The model has restrictions in that it is a turbulent viscosity model assuming the Boussinesq approximation. A derivation of the $k-\varepsilon$ model by the renormalisation approach show that the constant are not constants but there is no indication in the literature to suggest that this approach is any better for two-phase flow problems. For two phase flow problems, the energy spectrum has been shown to be quite different from single phase flow problems, particularly in the region where the buoyancy effects are significant. Liovic *et al.* (2003) using LES and Fulgosi *et al.* (2003) have shown that the enhanced energy decays according to the 8/3 power law seen in bubbly flow exist and confirms Lance and Bataille (1991) early experimental observation. Furthermore, the complete range of 5/3 to 8/3 energy decay power laws need to be predicted by a model in the bubbly region for the sub-inertial range. This cannot be predicted by any simple Class I or Class II (e.g. $k-\varepsilon$) turbulence model.

The calandria region is expected to be in such a bubbly flow regime and the advection of vapour bubbles into the upper and lower regions of the evaporator is likely to produce complex turbulent flow interactions. Currently the LES model requires 32 computers approximately two weeks to generate a few seconds of results for evaluation Liovic *et al.* (2003); the extension to an evaporator simulation is not likely for a few decades. The use of the $k-\varepsilon$ model is justified as it is a low Reynolds number turbulence model, is robust in its application, does allow the prediction of laminarisation (the original topic of the paper on the model itself), and the computing power required for an accurate turbulence model for two-phase flow is yet to come.

4.11 Convergence criteria

For both evaporators two convergence criteria were defined with the requirement that both must be satisfied before the simulation is complete. The root mean squared (RMS) residual errors for the momentum calculations in the three component directions, the additional variable calculations for sugar concentration and the energy calculations for heat flow had to be less than $1.0\text{x}10^{-4}$. In this case taking all of the residuals throughout the domain, squaring them, taking the mean and then taking the square root of the mean obtains the RMS residual error.

A second convergence criterion was also established as the overall mass balance defined as follows:

$$\dot{m}_{in} - \dot{m}_{out} - \dot{m}_e < 0.0001 \qquad \textbf{(4.23)}$$

In most cases the overall mass balance was the last criterion to be met due to its relatively small magnitude. However, it was found to be necessary to ensure accurate calculation of the sugar concentration at the outlet. Simulations where the mass balance criterion was not used showed significant error in the predicted sugar concentration at the outlet, even though the residuals target was satisfied.

4.12 Meshing of the geometry

The geometry of the vessel was modelled with a finite volume approach, using an unstructured mesh. Tetrahedral shaped mesh elements were used for a majority of the volume, with pyramidal and orthogonal shaped mesh elements used for those regions immediately adjacent to any external walls or internal walls with a no slip boundary condition applied. The different shaped objects at the wall were used to reduce the numerical diffusion problems commonly encountered with tetrahedral shaped mesh elements adjacent to walls. The number of orthogonal shaped mesh elements attached to any wall in all cases was five layers. The height of each layer varied slightly between cases depending on the estimated local velocity gradients that were checked after the first model was run.

The size of the mesh was found to be the single largest contributing factor to the usage of computer memory. As mentioned previously in this chapter, maximum advantage was taken of the symmetry of the vessels, in an attempt to reduce the size of the computational mesh.

4.12.1 Mesh independence

Before the majority of the modelling began a mesh independence test was conducted using the Proserpine #4 geometry. The one-quarter geometry model was created and all of the physics that were to be used in the final model were implemented. The only simplification applied to the physics was that 10% of the evaporation rate was applied instead of the full evaporation rate. The evaporation rate was reduced since it was found to be the one parameter that caused extended solution times. This was especially important in this case since the large mesh size being used increased solution times. All of the other physics associated with the model were included since it was believed that any further simplifications would prevent the mesh independence being an accurate representation of the model once it is applied in full.

Four different mesh densities were applied to the geometry, detailed as follows:

- the “coarse” mesh contained 24832 nodes,

- the "medium" mesh contained 239963 nodes,
- the "fine" mesh contained 324121 nodes, and
- the "very fine" mesh contained 532488 nodes.

The "very fine" mesh was used as a comparison for the other mesh densities. The "very fine" mesh simulation required a second computer running in parallel. The second computer was only available for a short period of time and could not be used for all modelling completed as part of this investigation. The "fine" mesh density was used for all subsequent modelling.

After the four simulations were completed the solution from the very fine mesh was compared with the solution from the coarse, medium and fine meshes. The predicted velocity and sugar concentration fields for the coarser meshes were interpolated onto the node locations of the fine mesh. The difference between the predictions was then calculated at each node location in the fine mesh. For each mesh comparison, the error was calculated with the L_2 norm error according to:

$$error = \sqrt{\frac{\sum_{i=1}^{n}(\Delta x)^2}{n}} \qquad (4.24)$$

Where x can be substituted for any variable and n is the number of mesh nodes.

The velocity and the sugar concentration variables were chosen as the two variables to use for comparison purposes. These variables were used since they were believed to be the two variables most likely to influence the predicted solution. The combined results of the mesh comparisons is displayed in

Table 4.3 Calculated errors from different mesh densities

Mesh	Number of nodes	Velocity error (m/s)	Brix error (%)
Course	24832	0.357	4.99×10^{-3}
Medium	239963	0.037	5.17×10^{-4}
Fine	324121	0.026	3.17×10^{-4}

Figure 4.2 is a plot of the velocity errors on a logarithmic scale and Figure 4.3 is a plot of the brix errors on a logarithmic scale.

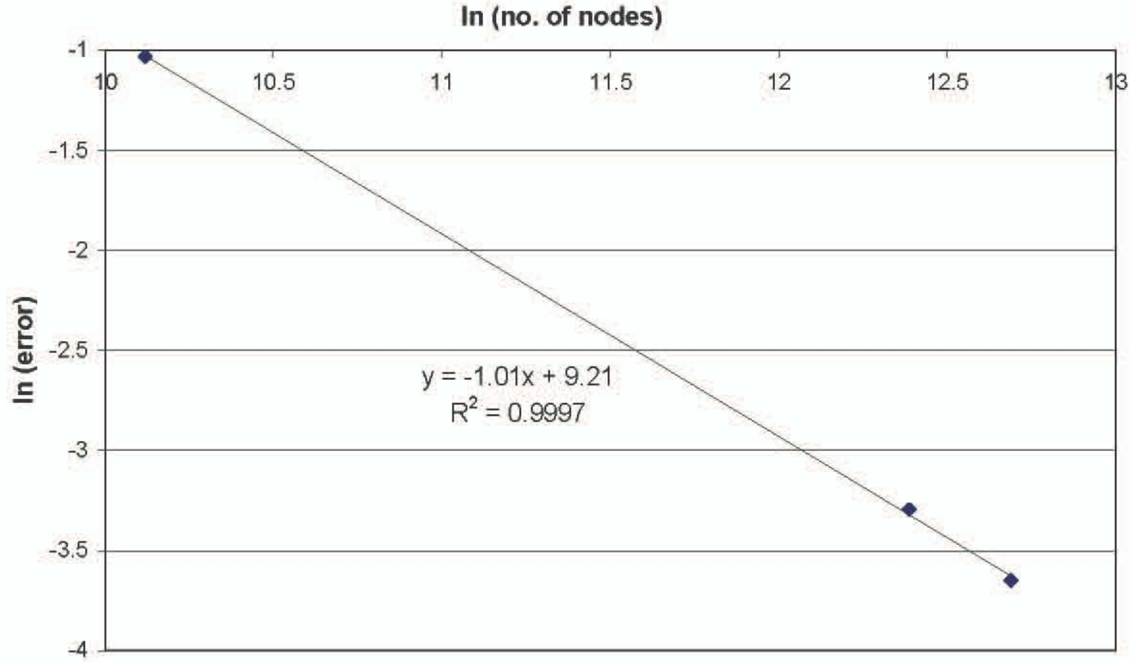

Figure 4.2 Plot of the velocity errors relative to the "very fine" mesh

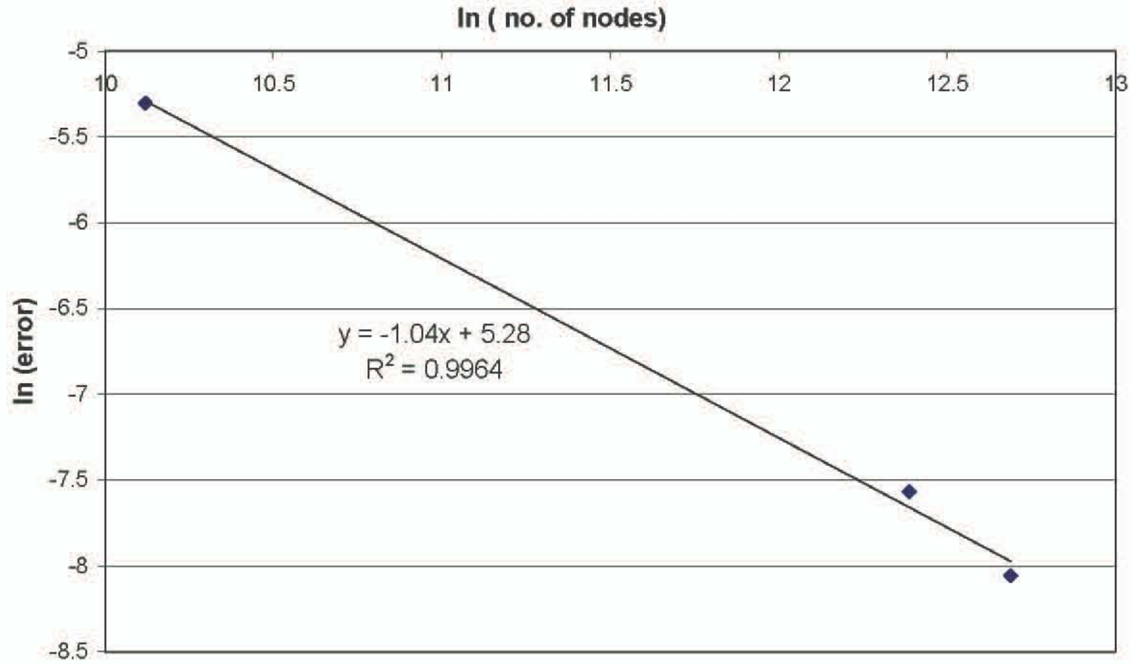

Figure 4.3 Plot of the brix errors relative to the "very fine" mesh

The slope from Figure 4.2 and Figure 4.3 is approximately -1, indicating first order convergence. Hence, the error will decrease by half for every doubling of the mesh density. As all the simulations at different mesh densities do converge, stability is not a problem. The "fine mesh" is expected to provide an error of $\pm 2.6\%$ relative to a mesh independent solution. Although the qualitative results in the subsequent solutions have a $\pm 2.6\%$ average error, the simulation results are expected to be qualitatively correct as the simulation is stable.

4.13 Summary of the numerical model

The complicated physics that occurs inside an evaporator requires some simplifying assumptions to be made so that a useful CFD model of the flow inside these vessels can be developed. The mathematical representation of the vertical heating tubes inside the calandria region have shown that it is possible to adequately account for the influence they have on the fluid flow in this calandria, without modelling each tube specifically.

Significant complexity was avoided by employing an Eulerian-Eulerian approach to the multi-phase nature of the fluid. The entire fluid was treated as a liquid with variations in density. Assuming zero slip between liquid and vapour allows for the average density and the resulting buoyancy forces to be calculated. Modelling of the bubble dynamics was not possible in this investigation since the fluid was assumed to be single phase. Modelling of the gaseous phase was not possible given the resources available for this investigation.

Mathematically modelling the heating tubes inside the calandria and taking advantage of symmetry were all steps taken to reduce the size of the computational mesh. In this study the available memory resources of the computer hardware were a limiting factor on the size of the computational mesh that could be used. In spite of efforts taken to reduce memory requirements, a mesh independence test showed that the model predictions are slightly mesh dependant. This must be taken into consideration when examining the results of model predictions produced as part of this study. However, the results are believed to be adequate enough to produce useful and realistic trends.

A suitable equation to describe the heat transfer process from stainless steel heating tubes to sugar solutions does not exist in the literature. A standard equation for describing the heat transfer process from a stainless steel heating surface to pure water has been applied. However, the form of the equation does allow for adaptation with further research, since it is in a form where the empirical constants can be modified to suit sugar solutions.

5. Model validation results

5.1 Introduction

Validation of the CFD model predictions is necessary to provide a means of judging the model's ability to reproduce the actual fluid flow behaviour inside evaporator vessels. As simplifications to the process are required for modelling, validation provides confirmation that the physics of the fluid flow has been adequately represented. If the model can accurately represent the physics then it can be applied as an engineering design tool.

Previous chapters of this thesis have described the factory data gathered and the equations used in the model. This chapter will provide a comparison between the predictions obtained from the model and the data gathered from the factory vessels. The result of this comparison will allow the accuracy of the CFD model developed to be quantified.

5.2 Validation procedure

The factory experiments provide juice brix and temperature measurements at strategic points in the region below the calandria as well as the total heat flow through the calandria. The validation was performed in two steps; 1) validating the juice brix and temperature at strategic points, and 2) validating the heat flow through the calandria.

For the first validation step, the heat flow through the calandria was applied as a boundary condition equal in magnitude to the value provided from the factory experiments. This procedure was performed as a means of simplifying the model. By fixing the heat flows through the calandria the calculations required for the overall heat balance on the vessel were simplified and the energy equations were de-coupled from the brix and temperature predictions. Equation (4.18) includes a number of terms that are a function of the juice brix and temperature and replacing this equation with a constant value provided faster convergence and ensured that the heat flow through the calandria was the same as the value provided by the factory experiments.

For the second validation step, the heat flow through the calandria was calculated according to equation (4.18), with the initial guess for the solution being set to the final solution obtained from the first validation step.

5.3 Validating the juice brix and temperature distribution

The results from all of the four tests conducted on the Proserpine #4 vessel and the six tests conducted on the Farleigh #2 vessel were used for validation. The complete data set has been given in Chapter 3 (Table 3.3 and Table 3.4); this chapter includes only the juice brix and temperature data used for validation purposes. Table 5.1 and Table 5.2 show the comparisons between the measured and predicted juice temperature data from the Proserpine #4 and the Farleigh #2 vessels respectively. The magnitude of the difference between the measured and the predicted juice temperatures is reported, along with the difference expressed as a percentage of the temperature difference between the steam and the juice at the time of testing. The difference between the measured and predicted temperature values was expressed as a percentage of the temperature difference because the absolute magnitude of the juice temperatures is significantly larger than the small differences in temperature required for adequate validation. The effective temperature difference also changes from one factory experiment to the next and allows for the changes in operating conditions to be accounted for.

Table 5.1 Measured and predicted juice temperature data from the Proserpine #4 vessel

	Measured (°C)	Predicted (°C)	Difference (°C)	Difference (%)
Test No. 1				
Point A	55.1	55.8	+0.7	+2.2
Point B	55.0	55.8	+0.8	+2.5
Point C	57.0	55.9	-1.1	-3.5
Test No. 2				
Point A	55.5	55.9	+0.4	+1.2
Point B	55.1	56.0	+0.9	+2.8
Point C	57.3	56.0	-1.3	-4.0
Test No. 3				
Point A	57.6	57.7	+0.1	+0.4
Point B	56.0	58.0	+2.0	+8.7
Point C	58.8	58.0	-0.8	-3.5
Test No. 4				
Point A	58.0	58.0	-0.03	-0.1
Point B	57.3	58.2	+0.9	+4.0
Point C	58.8	58.3	-0.5	-2.2

Table 5.2 Measured and predicted juice temperature data from the Farleigh #2 vessel

	Measured (°C)	Predicted (°C)	Difference (°C)	Difference (%)
Test No. 1				
Point A	98.4	100.1	+1.7	+26.6
Point B	97.3	100.2	+2.9	+45.3
Point C	n/a	n/a	n/a	n/a
Test No. 2				
Point A	98.5	100.1	+1.6	+24.6
Point B	97.2	100.1	+2.9	+44.6
Point C	95.0	100.1	+5.0	+76.9
Test No. 3				
Point A	91.9	96.2	+4.3	+75.4
Point B	91.3	96.3	+5.0	+87.7
Point C	90.2	96.3	+6.1	+107
Test No. 4				
Point A	93.3	95.4	+2.1	+32.8
Point B	92.6	95.5	+2.9	+45.3
Point C	92.3	95.5	+3.2	+50.0
Test No. 5				
Point A	92.2	96.9	+4.7	+75.8
Point B	92.4	97.0	+4.6	+74.2
Point C	93.1	97.0	+3.9	+62.9
Test No. 6				
Point A	95.2	97.2	+2.0	+33.8
Point B	94.0	97.3	+3.3	+55.9
Point C	94.7	97.3	+2.6	+44.1

The juice temperature predictions from the Proserpine #4 vessel show close agreement with the measured values, but the predictions from the Farleigh #2 vessel show significant variations in both absolute magnitude and in percentage terms. Some possible explanations for this difference are as follows:

- It is possible that the factory experiments were unable to measure the juice temperature to the level of accuracy required for very detailed comparisons,
- The model developed as part of this study is more suited for vessels operating with higher juice brix, and
- The physical differences between the Proserpine #4 calandria and the Farleigh #2 calandria are causing the fluid to behave differently and this behaviour is not being captured by the model predictions.

Table 5.3 and Table 5.4 show the comparisons between the measured and predicted juice brix data from the Proserpine #4 and the Farleigh #2 vessels respectively. The magnitude of the difference between the measured and predicted juice brix is reported, along with the difference expressed as a percentage of the juice brix change from inlet to outlet. These data were included because the change in juice brix from inlet to outlet can be quite small, particularly for early effect vessels such as the Farleigh #2.

Table 5.3 Measured and predicted juice brix data from the Proserpine #4 vessel

	Measured (%-wt)	Predicted (%-wt)	Difference (%-wt)	Difference (%)
Test No. 1				
Point A	63.5	61.4	-2.1	-7.7
Point B	65.0	61.9	-3.1	-11.4
Point C	63.6	62.4	-1.2	-4.5
Test No. 2				
Point A	64.4	61.7	-2.7	-9.8
Point B	65.7	62.4	-3.3	-11.9
Point C	64.5	62.9	-1.6	-5.9
Test No. 3				
Point A	68.5	64.5	-4.0	-13.5
Point B	72.9	66.7	-6.2	-20.9
Point C	67.1	66.9	-0.2	-0.7
Test No. 4				
Point A	68.1	64.2	-3.9	-13.5
Point B	69.1	66.2	-2.9	-9.9
Point C	66.7	66.6	-0.1	-0.4

Table 5.4 Measured and predicted juice brix data from the Farleigh #2 vessel

	Measured (%-wt)	Predicted (%-wt)	Difference (%-wt)	Difference (%)
Test No. 1				
Point A	28.3	25.9	-2.4	-58.3
Point B	27.4	26.0	-1.4	-33.6
Point C	n/a	n/a	n/a	n/a
Test No. 2				
Point A	27.1	25.2	-1.9	-48.7
Point B	26.4	25.2	-1.2	-30.5
Point C	n/a	25.1	n/a	n/a
Test No. 3				
Point A	n/a	27.2	n/a	n/a
Point B	28.7	27.4	-1.3	-32.2
Point C	27.5	27.4	-0.1	-2.4
Test No. 4				
Point A	n/a	26.5	n/a	n/a
Point B	27.5	26.7	-0.8	-18.0
Point C	26.4	26.8	+0.4	+8.1
Test No. 5				
Point A	n/a	25.5	n/a	n/a
Point B	26.9	25.7	-1.2	-29.0

Point C	26.0	25.8	-0.2	-5.8
Test No. 6				
Point A	n/a	25.8	n/a	n/a
Point B	27.2	26.1	-1.1	-27.0
Point C	26.4	26.1	-0.3	-6.5

The juice brix predictions for both the Proserpine #4 and the Farleigh #2 vessels show reasonable agreement with the corresponding measured values, except for the first two tests conducted on the Farleigh #2. This difference is likely caused by the location of the sampling points, as is discussed later.

5.4 Discussion of the juice brix and temperature validation

The predicted juice brix distribution for the Proserpine #4 vessel shows reasonably close agreement with the measured data. The largest difference being –20.9% for point B during test number 3. For all other points the difference between measured and predicted data is less than –13.5%. It must be noted that only point B in test number 1 was located above the bottom tube-plate of the calandria i.e., inside the heating tubes. While the data from the Proserpine #4 vessel shows reasonable agreement between measured and predicted values, it can only be considered an indication of the flow in the region below the bottom tube-plate. The flow behaviour inside the calandria is likely to be significantly different due to the complexity of the physical processes occurring in this region. This is a significant limitation in these validation data due to the number of simplifying assumptions that have been made in order to model the calandria section.

The predicted juice brix distribution for the Farleigh #2 vessel shows larger differences from the measured values, in particular tests number 1 and 2. However, the location of the sampling points for both of these tests is above the bottom tube-plate of the calandria. Due to the size of the sampling probe being only slightly smaller than the heating tube itself it is possible that the presence of the sampling probe in these locations has adversely affected the fluid flow. If this is the case then it is likely that the measured data will be significantly different to the predicted data.

The remainder of the data from the Farleigh #2 vessel are located in the region below the calandria and show reasonable agreement between the measured and predicted values. Even though some of the differences are larger than those from the Proserpine #4 vessel the juice brix predictions in the region below the calandria are still considered acceptable.

The data shows that in almost all cases the juice brix is under predicted for both vessels, but the juice temperature is over predicted. This is a strange result since an under predicted juice brix would result in an under predicted boiling point elevation temperature. If this were the case then the juice temperature would also be under predicted. The cause of this difference is the magnitude of the juice temperature at the inlet. This boundary condition was determined directly from the factory measurements. It is possible that this temperature was measured incorrectly during the experiments and the associated error has followed on to the model predictions. Since the variation in juice temperature any errors in the juice temperature boundary condition applied at the inlet will have a significant effect on the predicted juice temperature distribution throughout the vessel.

The predicted juice brix and temperature data shows good agreement with the measured data in general terms and the observed trends have been predicted reasonably accurately. The range of processing conditions covered during the factory experiments was sufficient to cover a majority of the conditions normally experienced in an evaporator set with a large difference in the operating temperatures of the two vessels. The model applied to both vessels was exactly the same with no arbitrary constants or empirical values used in either case. This supports the accuracy of the predictions in general terms even though it must be recognised that some differences exist between the absolute magnitude of the juice brix and temperature predictions, when the heat flow through the calandria is applied as a boundary condition.

5.5 Validating the heat flow predictions

The processing conditions experienced during factory testing were all applied as boundary conditions to the CFD model during the validation procedures for the juice brix and temperature. When validating the heat flow predictions the boundary condition was replaced by the expression detailed in equation (4.18), and the measured heat flow was used for comparison purposes. For comparison purposes the values displayed as the heat required for evaporation from Table 3.5 and Table 3.6 have been used as the measured values. The magnitude of the difference between the measured and predicted values is expressed as a percentage of the measured value.

Table 5.5 Measured and predicted heat flow data from the Proserpine #4 vessel

	Measured (MW)	Predicted (MW)	Difference (%)
Test No. 1	73.52	64.90	-11.7
Test No. 2	75.02	65.30	-13.0
Test No. 3	82.18	49.15	-40.2
Test No. 4	80.72	48.06	-40.5

Table 5.6 Measured and predicted heat flow data from the Farleigh #2 vessel

	Measured (MW)	Predicted (MW)	Difference (%)
Test No. 1	30.59	37.60	+22.9
Test No. 2	26.41	39.44	+49.3
Test No. 3	22.12	21.89	-1.0
Test No. 4	26.07	31.53	+20.9
Test No. 5	30.12	33.14	+10.0
Test No. 6	29.93	29.15	-2.6

The results of comparison between the measured and the predicted heat flows show varying levels of success. The heat flows in the Proserpine #4 vessel is always under predicted, but is within acceptable limits for the first two tests. However, there is a predicted decrease in heat flow for the second two tests and this change is in the opposite direction to the measured data. When considering tests numbers 3 and 4 were conducted immediately after the evaporator was cleaned, the data would indicate that the effect of cleaning is not being captured. However, the same behaviour is not displayed in the Farleigh #2 data. In this case the two tests conducted after the evaporator was cleaned (test numbers 5 and 6) show good agreement between the measured and the predicted heat flows. Also, the heat flow in the Farleigh #2 vessel is over predicted for the tests conducted before the evaporator was cleaned. This can be explained by because the Rohsenow (1952) equation (4.18) was developed for clean heating surfaces. These results indicate that a modification of the constants within equation (4.18) is required to take into account the effect of fouling. As this can only be completed experimentally it was considered outside the scope of this investigation.

Table 5.6 shows that the heat flow prediction from the Farleigh #2 vessel are all within acceptable limits, except for test number 2. If this outlier is neglected then all predictions are within +22.9% of the measured value.

The results of the heat flow validation analysis are encouraging when the form of the expression used to predict the heat flow is considered. This expression was developed for heat transfer between stainless steel surfaces and clean water. The fact that the properties of sugar solutions can vary significantly from those of water, particularly at high concentrations, was known before the expression was applied. Also, the magnitudes of the constants substituted into the expression were derived empirically for stainless steel and water. These results would indicate that the form of the expression used is likely to be correct and the direction of future research should be focussed on refinement of the constants used.

The results of the analyses completed during this study also indicate that an allowance for the amount of fouling on the heating tubes needs to be considered, particularly for latter effects in the set.

5.6 Summary of the model validation results

When the heat flow through the calandria is applied as a boundary condition, the predicted juice brix distribution in the region below the calandria shows good agreement with the measured data. Reduced accuracy has been identified in the juice temperature predictions for a calandria without downtakes. It is possible that different simplifying assumptions are required to model a calandria without downtakes. The development of such a model is considered to be outside the scope of this study and the resulting errors are identified but are acceptable for the purpose of this study.

On average, the heat flow through the calandria is always under predicted on for the Proserpine #4 vessel and over predicted for the Farleigh #2 vessel. The predicted heat flows are generally within acceptable limits, with a small number of outliers. However, the effect of evaporator cleaning does not appear to be captured. This is to be expected since the expression used to calculate the predicted heat flow was developed for a clean heating surface and clean water. The results of this validation indicate that the direction of future research should be focussed on refinement of the constants used.

6. Model prediction results

6.1 Introduction

Chapter 5 described the comparison between the measured data and model predictions to determine accuracy. This chapter describes the predicted behaviour of the flow fields within the evaporator and possible methods to improve the design of the Roberts evaporator.

For the case of the Proserpine #4 and the Farleigh #2 vessels, four and six operating conditions respectively were modelled. These conditions correspond to the operating conditions of the vessel at the time each factory experiment was carried out and did not vary significantly.

Proserpine #4:

- juice concentration at inlet, 35.6 to 38.1%,
- juice flow rate at inlet, 289.8 to 311.1 $t{\cdot}h^{-1}$, and
- heat flow through the calandria, 73.5 to 82.2 MW.

Farleigh #2:

- juice concentration at inlet, 21.7 to 23.9%,
- juice flow rate at inlet, 277.7 to 328.9 $t{\cdot}h^{-1}$, and
- heat flow through the calandria 22.1 to 30.6 MW.

The CFD predictions were subsequently found to be insensitive over these ranges. Only the conditions from Proserpine test #1 and from Farleigh test #1 have been used in this chapter as a representative result from each vessel, and will be discussed in sections 6.2 and 6.3.

After examining the results from the modelling of the existing Proserpine #4 and Farleigh #2 geometries, modifications to the existing design and a novel design were modelled. The modifications discussed in section 6.5 were applied to the Farleigh #2 geometry and showed limited improvement to the flow field and to the predicted heat transfer. A novel, linear design was then developed and modelling of this geometry was then carried out.

Significant improvement in the flow field behaviour and the predicted heat transfer performance are observed for the novel design and is discussed in section 6.6.

6.2 Proserpine #4

6.2.1 CFD model details

The geometry of the Proserpine #4 vessels displays 1/4 symmetry and was modelled using a 90° wedge and two planes of symmetry. A mesh containing 413966 nodes was applied to the geometry. The mesh density in the region below the calandria and in the calandria itself was set reasonably coarse (Figure 6.1) but the mesh in the area around the juice inlet and inside the downtakes was set finer. Results from initial modelling showed that the largest velocity gradients occurred in the region around the juice inlet and the deflector plate. Velocity gradients inside the downtakes were also found to be significant.

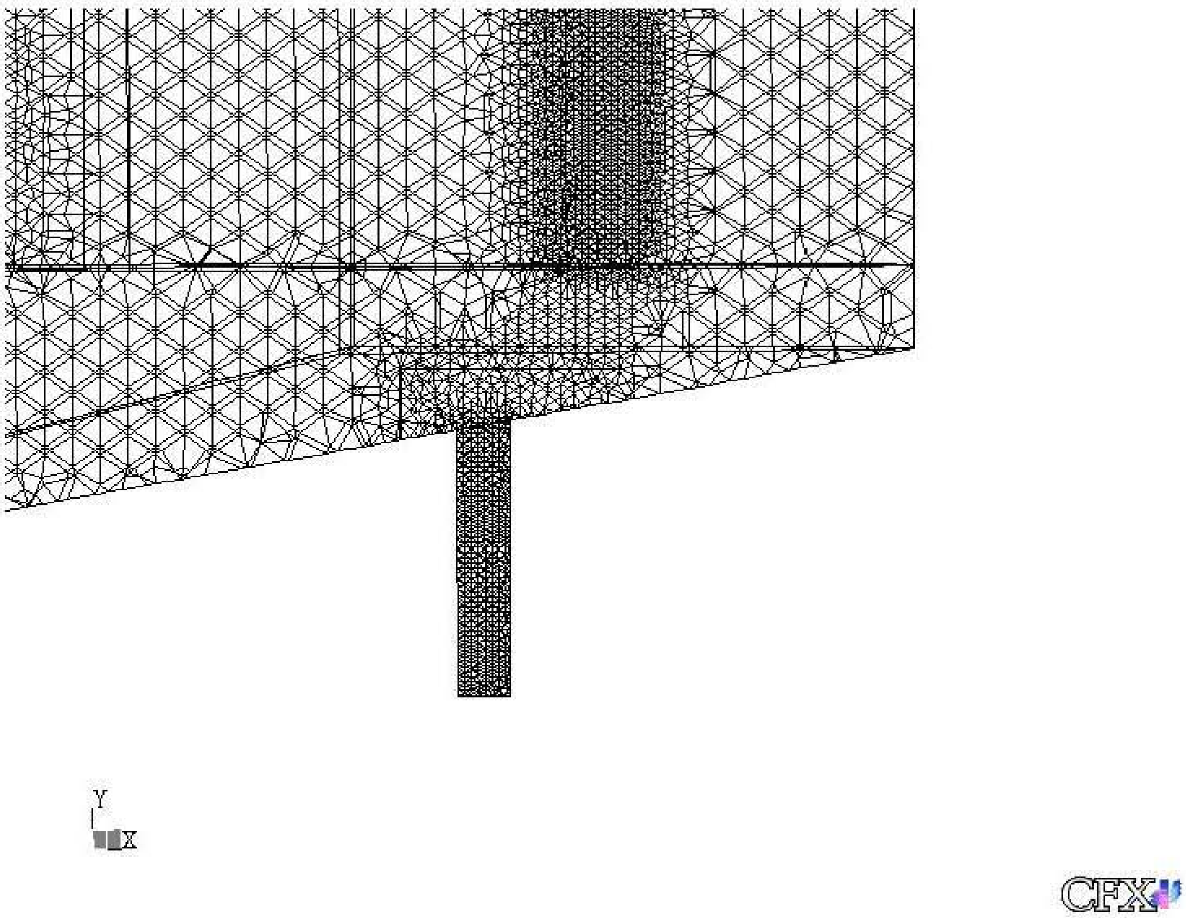

Figure 6.1 Mesh applied to the Proserpine #4 geometry

6.2.2 Circulation patterns

One of the assumptions made in the development of the model was the method used to model the flow in the vertical heating tubes inside the calandria. In the case of the Proserpine #4 vessel the juice flow through the heating tubes is vertically up, small in absolute magnitude and has minimal sideways movement. The flow in the downtakes is always in the downward direction and larger in magnitude than the upward flow in the heating tubes. The flow in the regions above and below the calandria is slow moving with no defined flow pattern. Figure 6.2 shows a vector plot on a vertical plane running through the centre of the vessel and passing through the centre of one of the juice inlet pipes. The vector length is proportional to the magnitude of the velocity and shows the slow moving fluid flowing up the calandria tubes and the fast moving fluid flowing down the downtake. The irregular vector spacing is caused by the unstructured mesh.

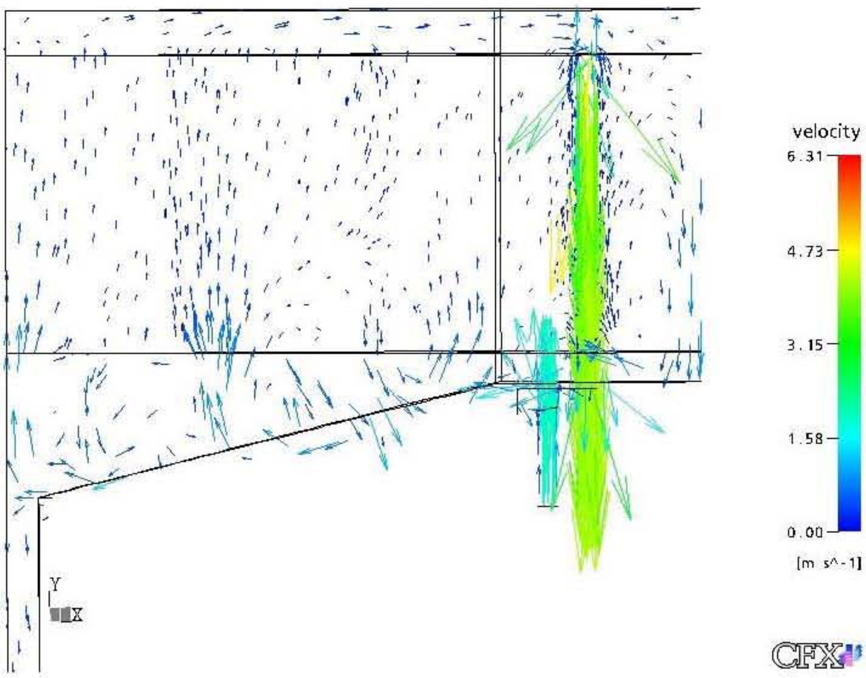

Figure 6.2 Vector plot on a vertical plane through the centre of one of the juice inlets for the Proserpine #4 vessel

The juice flow in the immediate vicinity of the juice inlet is mixed by a large volume of down flow at high concentration and this is influencing the flow in the remainder of the vessel. Figure 6.3 shows a close up of the juice flow around the inlet, as shown in Figure 6.2.

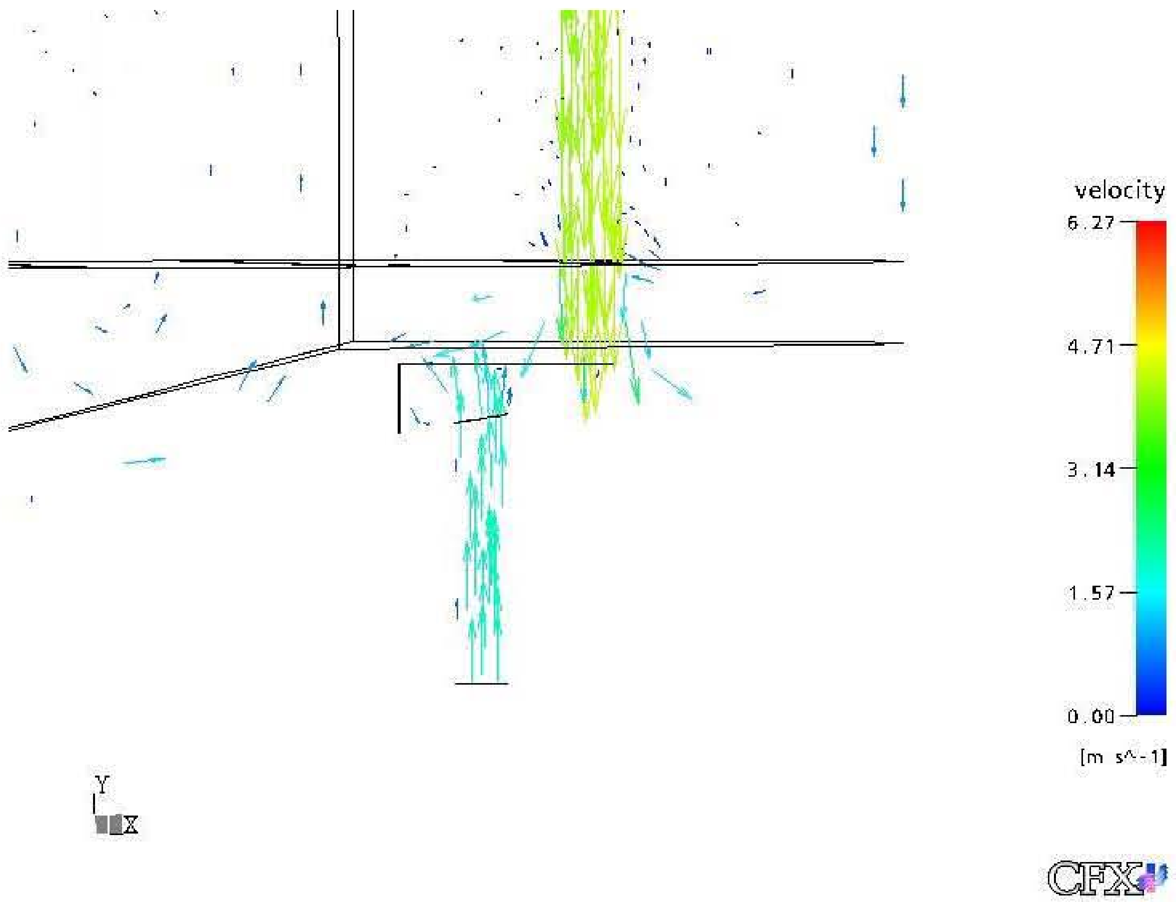

Figure 6.3 Close up vector plot of the juice flow around the inlet from Figure 6.2

For the representative case, the mass flow rate of high brix juice flowing down the downtake is 95 $kg \cdot s^{-1}$ and the mass flow rate of low brix juice flowing in through the inlet is 20 $kg \cdot s^{-1}$. With almost four times the quantity of high brix juice mixing with the inlet juice, the mixing occurs within a very short distance of the vessel's inlet.

Since this mixing is occurring in the immediate vicinity of the distribution plate, the low brix juice flowing into the vessel does not have the chance to contact the heating tubes directly. Instead the inflowing juice is mixed and is at significantly higher brix by the time it reaches the heating tubes. This behaviour is detrimental to the heat transfer performance of the vessel since the higher brix juice is harder to boil. This mixing is further supported by Figure 6.4 which is a plot of juice brix in the same vertical plane as Figure 6.2.

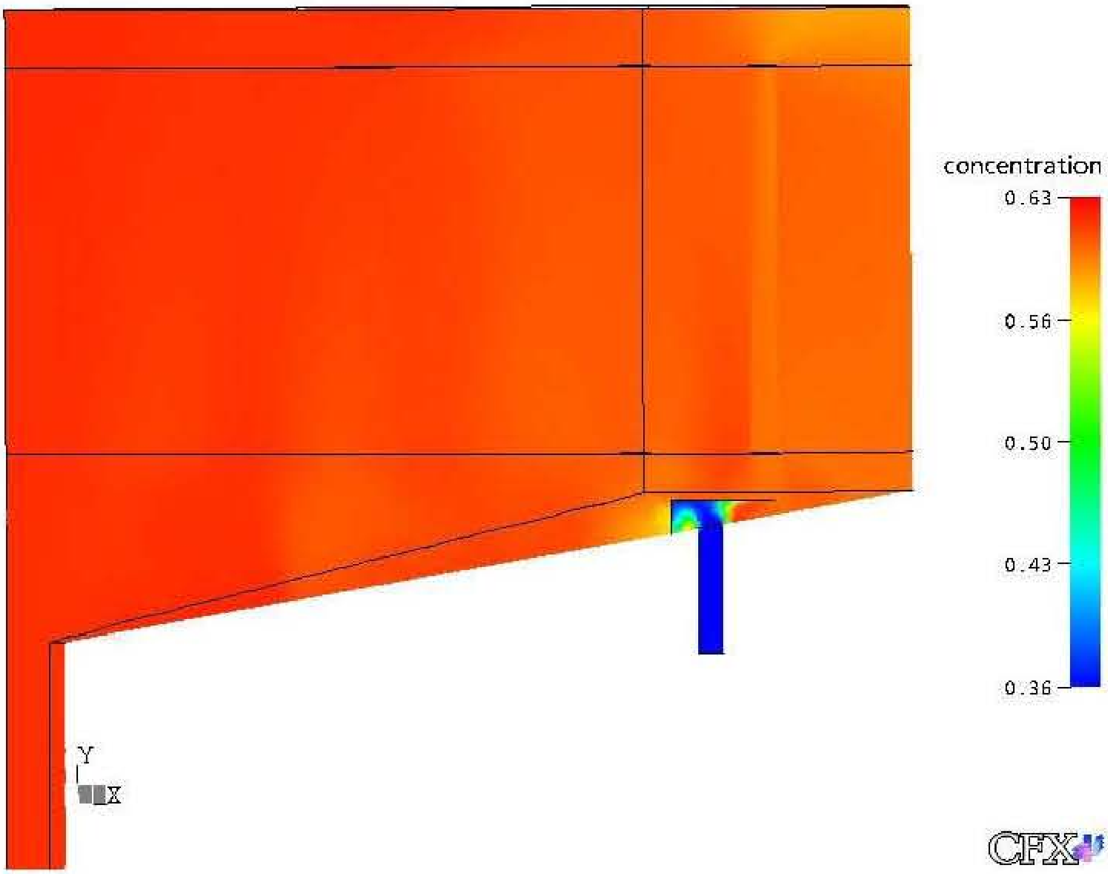

Figure 6.4 Juice brix plot on a vertical plane through the centre of one juice inlet for the Proserpine #4 vessel

Figure 6.4 shows that a majority of the juice inside the vessel is at relatively high brix, comparable to the outlet, with only the juice in the immediate vicinity of the juice inlet pipe at relatively low brix. Figure 6.4 shows the large gradients in juice brix in the vicinity of the distribution plate caused by the mixing action occurring in this region. Figure 6.5 is a plot in a horizontal plane located 50 mm below the distribution plate. This figure shows the localised areas of low brix juice in the immediate vicinity of the inlet, also shown is the locations of the downtakes. A point to note is the location of one of the downtakes is almost directly above the distribution plate. High brix juice flows from the region above the calandria almost directly into the inlet juice stream.

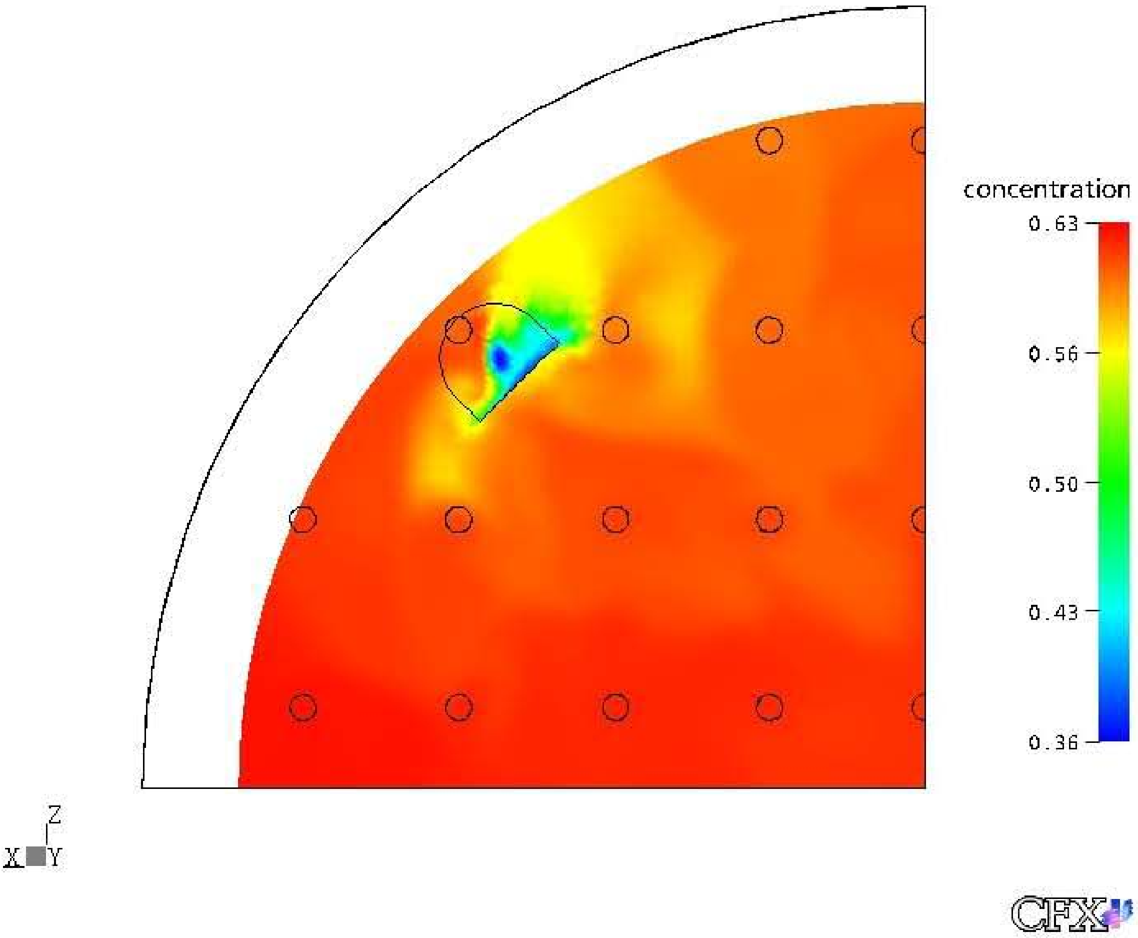

Figure 6.5 Juice brix plot on a horizontal plane 50 mm below the distribution plate for the Proserpine #4 vessel

Figure 6.5 shows the location of the downtakes in relation to the juice inlet pipe and the distribution plate. A number of the downtakes are located very close to the juice inlet and one is situated almost immediately above. There is potential to improve the circulation pattern inside the vessel by moving the downtakes away from the inlet so that the high brix juice flowing down the downtakes is away from the low brix juice at the inlet.

The total quantity of juice flowing into the vessel is 290 $t{\cdot}h^{-1}$ with 164 $t{\cdot}h^{-1}$ flowing out and 126 $t{\cdot}h^{-1}$ of water is evaporated and flows out of the vessel as vapour. The total amount of juice flowing down all of the downtakes in the vessel is approximately 19 000 $t{\cdot}h^{-1}$ or 66 times the amount of juice flowing into the vessel. The amount of energy required to move such large quantities of fluid around the inside of the vessel is extremely wasteful. The large quantity of juice being recirculated around also helps to explain why the vessel is so well mixed.

6.2.3 Residence time distribution

The poor circulation patterns predicted by the CFD model highlighted the possible need for further confirmation of this behaviour by factory data. Pennisi (2002) details a tracer test that was conducted on the Proserpine #4 vessel and the residence time distribution (RTD) plot that was produced as a result of that test. The tabulated data and the RTD plot have been included in Appendix D. Over 90% of the total tracer injected into the inlet was recovered at the outlet.

Figure D 1 shows the RTD plot where large concentrations of tracer were detected at the outlet approximately two minutes after injection at the inlet. The concentration spikes occur randomly for approximately 15 minutes and the entire tracer leaves the system before the mean residence time of 23 minutes. Observations that can be made from this result are as follows:

- A sharp concentration spike is recorded within two minutes of tracer injection, compared to the mean residence time of 23 minutes. This indicates that the vessel displays extensive bypass;
- The entire tracer exits the vessel earlier than the mean residence time. This indicates that the juice flowing through the inlet is mixed early and is then pushed towards the outlet as a slug. This is an operational deficiency with poor mixing of the juice flowing in the inlet and the juice in the remainder of the vessel. This must be fixed to promote better utilisation of the entire evaporator vessel;
- The spiky nature of the RTD suggests the flow is consistent with a channelling type flow; and
- The interaction between the bulk of the juice inside the evaporator and the inlet juice is minimal.

The tracer test and RTD data provides a critical link between the factory data and the CFD model predictions since it gives a description of the flow behaviour inside the entire vessel rather than simply at strategic points in the juice space under the calandria. The RTD data describes the mixing of juice that occurs in the region of the inlet and this can be directly compared to the CFD model predictions.

Unfortunately a similar tracer test was not conducted on the Farleigh #2 vessel.

6.3 Farleigh #2

6.3.1 CFD model details

The geometry of the Farleigh #2 vessels displays 1/2 symmetry and one half of the vessel was modelled using one plane of symmetry. A mesh containing 323182 nodes was applied to the geometry. The mesh density in the region below the calandria and in the calandria itself was set reasonably coarse (Figure 6.6) but the mesh in the area around the juice inlet was set finer. Experience from the modelling of the Proserpine #4 vessel showed that the region around the inlet was most likely to have the largest velocity gradients; this was later found to be true.

The density of the mesh inside the calandria section of the Farleigh #2 vessel is finer than that of the Proserpine #4. This is because the calandria is physically smaller and no downtakes are fitted. The absence of downtakes provides a more problematic difficult flow pattern to model since there is no defined flow path and the juice must flow down some of the heating tubes.

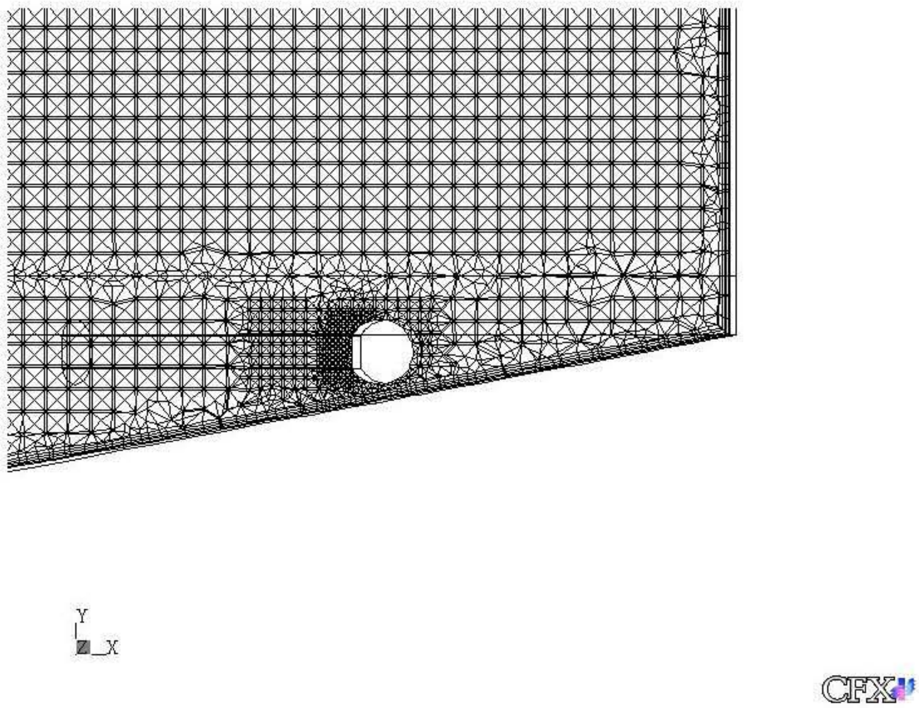

Figure 6.6 Mesh applied to the Farleigh #2 geometry

6.3.2 Circulation patterns

The juice flow through the heating tubes of the Farleigh #2 vessel is restricted to the vertical direction but does not have the defined flow path of up the heating tubes and down the downtakes like the Proserpine #4. Since the Farleigh #2 vessel is a much older design and does not have downtakes fitted, the juice must flow down some of the heating tubes in order to reach the outlet. By flowing down the heating tubes the juice effectively reduces the heating surface area of the vessel by suppressing the boiling action in those tubes. Figure 6.7 is a vector plot on a vertical plane, parallel to the plane of symmetry that runs through the centre of one of the juice outlet pipes. It shows that the juice has a portion of tubes immediately above the juice inlet where the juice flows down the heating tubes.

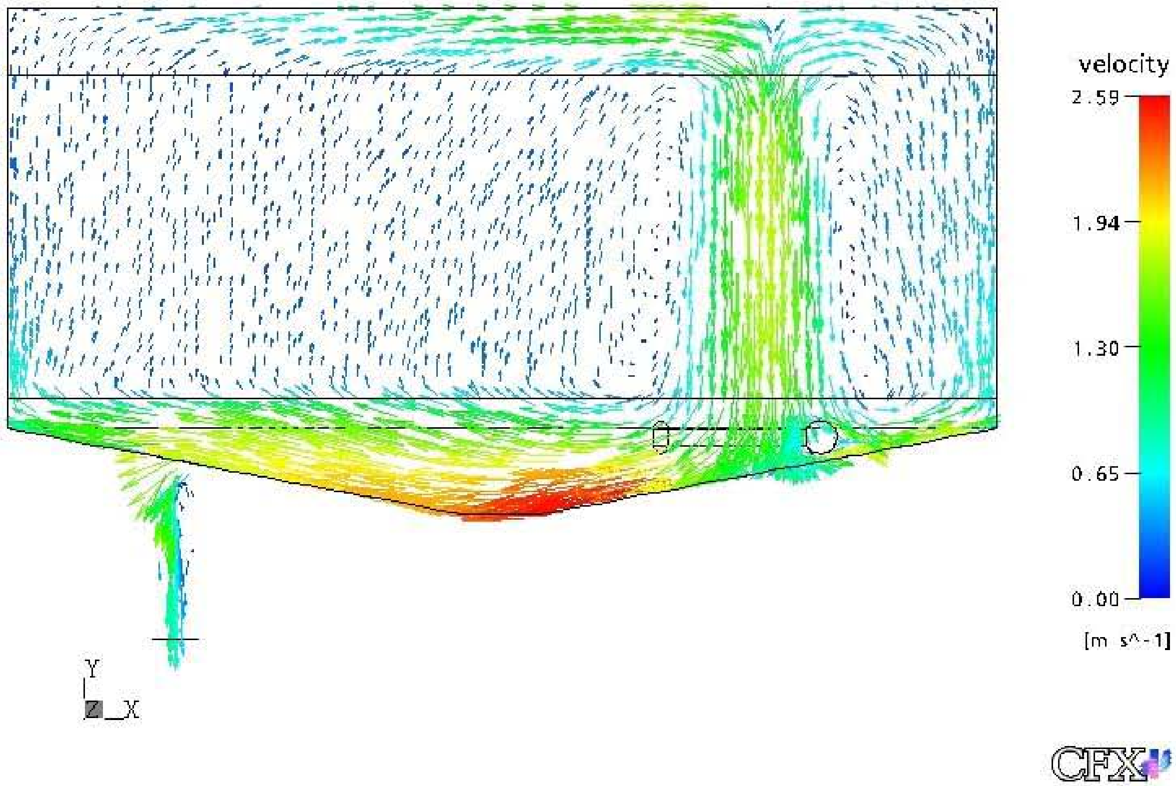

Figure 6.7 Vector plot on a vertical plane through the centre of one of the juice outlets for the Farleigh #2 vessel

The velocity plots shows that the jet formed by the juice flowing horizontally from the inlet entrains fluid from the surrounding region. Figure 6.8 shows that the entrainment subsequently creates a region of low pressure in the region below the heating tubes. This explains why there is still downflow in the calandria where there is no downtakes fitted and why this downflow is occurring in those tubes immediately above the juice inlet manifold. In this manner the flow field inside the Farleigh #2 vessel is very similar to the Proserpine

#4 where the juice flowing through the inlet of the vessel mixes with juice flowing down through the calandria from directly above the juice inlet location.

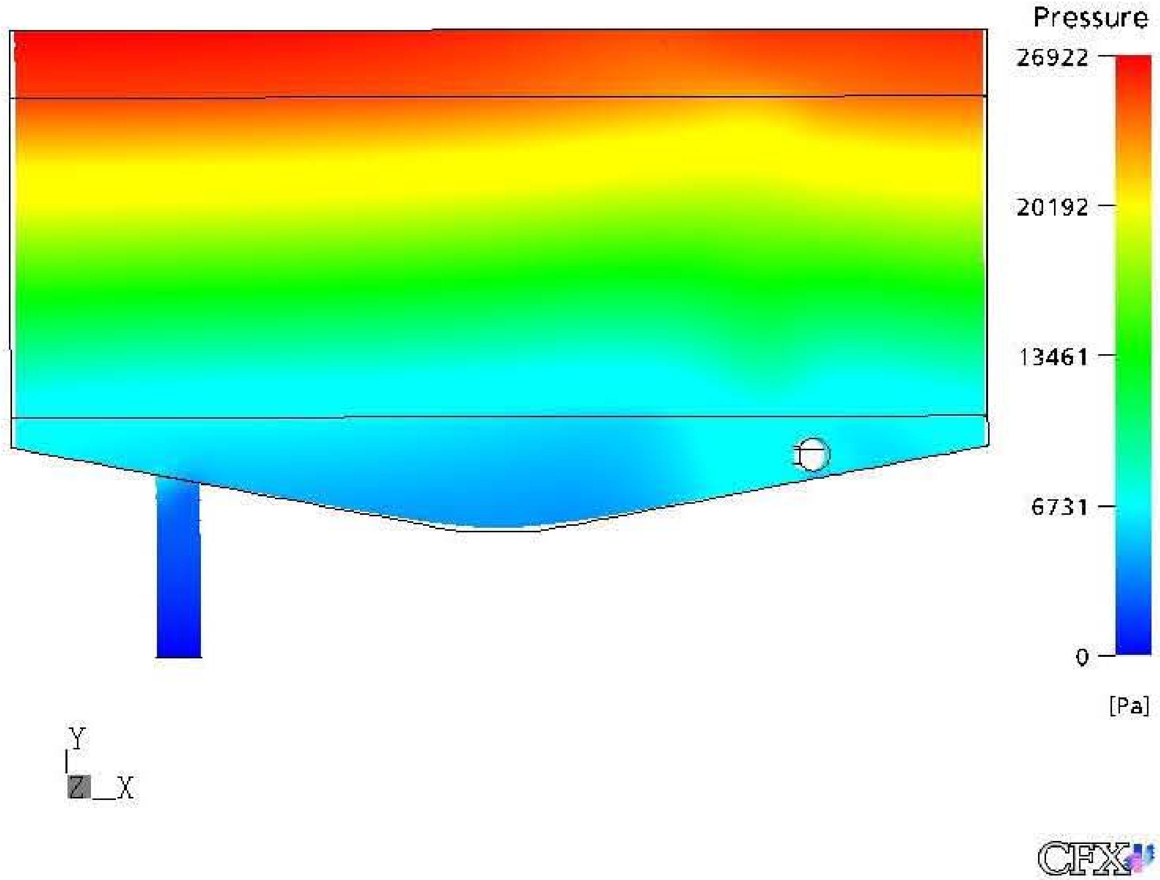

Figure 6.8 Pressure plot on a vertical plane through the centre of one of the juice outlets for the Farleigh #2 vessel

The flow pattern described by Figure 6.7 produces a large amount of mixing in the immediate vicinity of the juice inlet pipe. The high brix juice flowing from the region above the calandria flows down the heating tubes and mixes with the low brix juice flowing in from the inlet. Since this mixing is occurring in the immediate vicinity of the juice inlet pipe, the low brix material flowing into the vessel does not have the chance to contact the heating tubes directly. This behaviour is similar to that observed in the Proserpine #4 vessel and the detrimental effects have already been discussed for that vessel. Figure 6.9 shows a close up of the mixing action around the juice inlet.

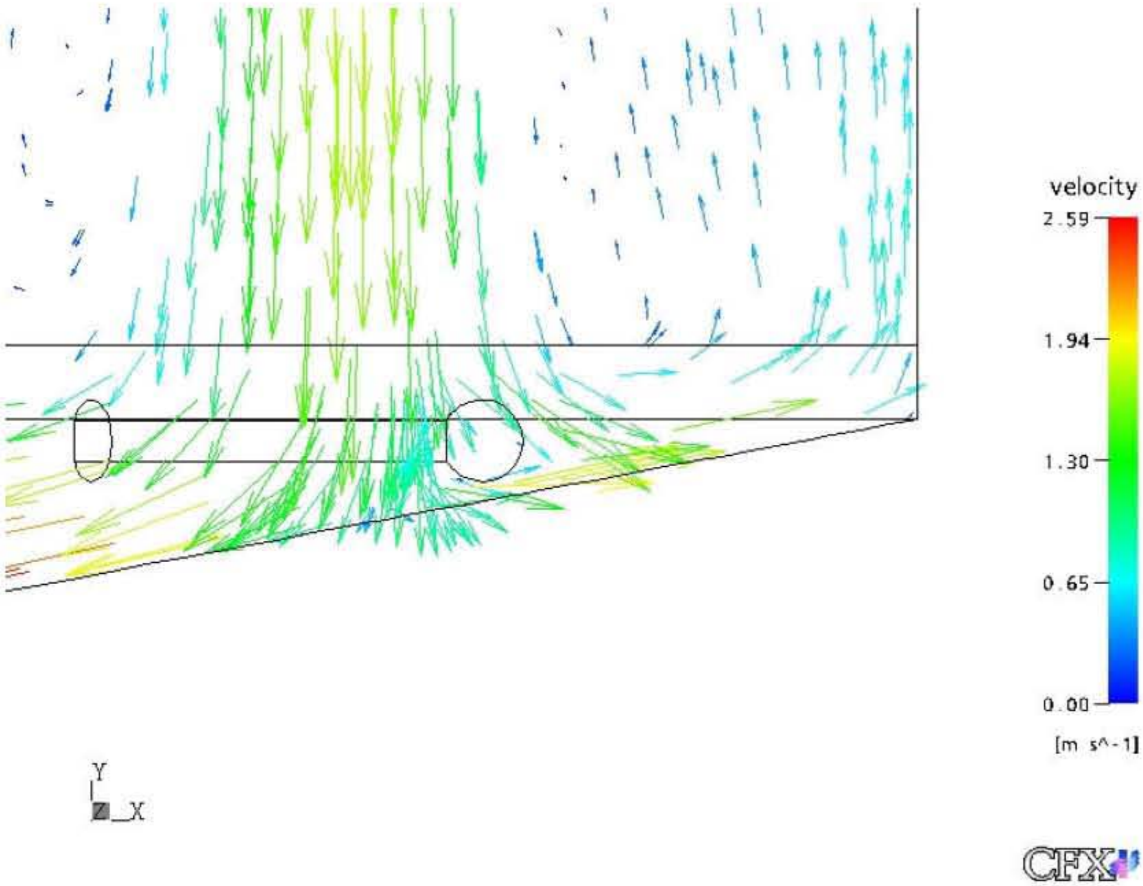

Figure 6.9 Close up vector plot of the juice flow around the inlet from Figure 6.7

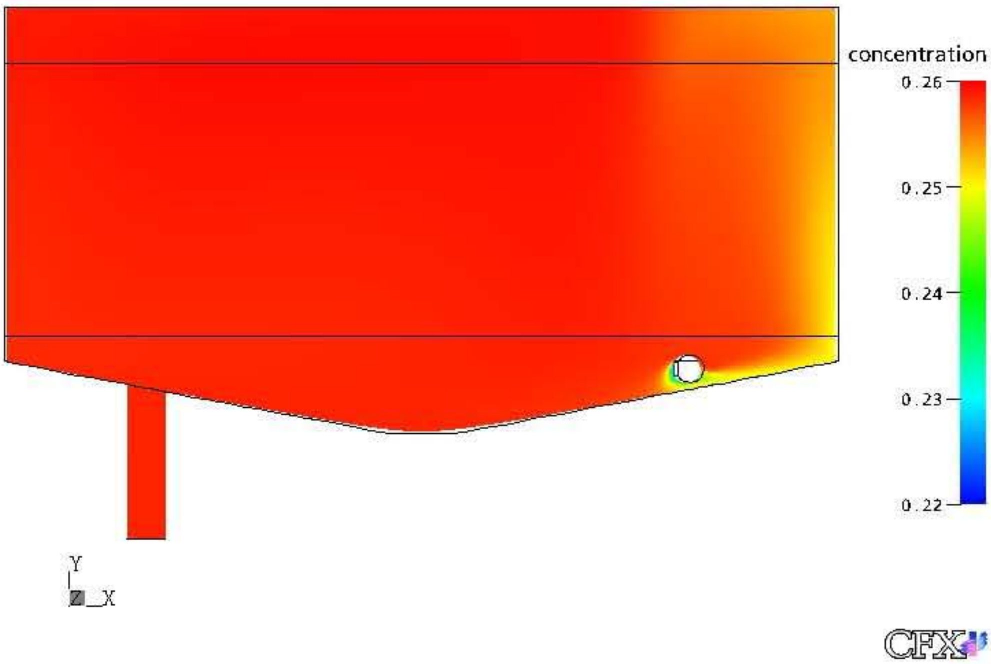

Figure 6.10 Juice brix plot on a vertical plane through the centre of one of the juice outlets for the Farleigh #2 vessel

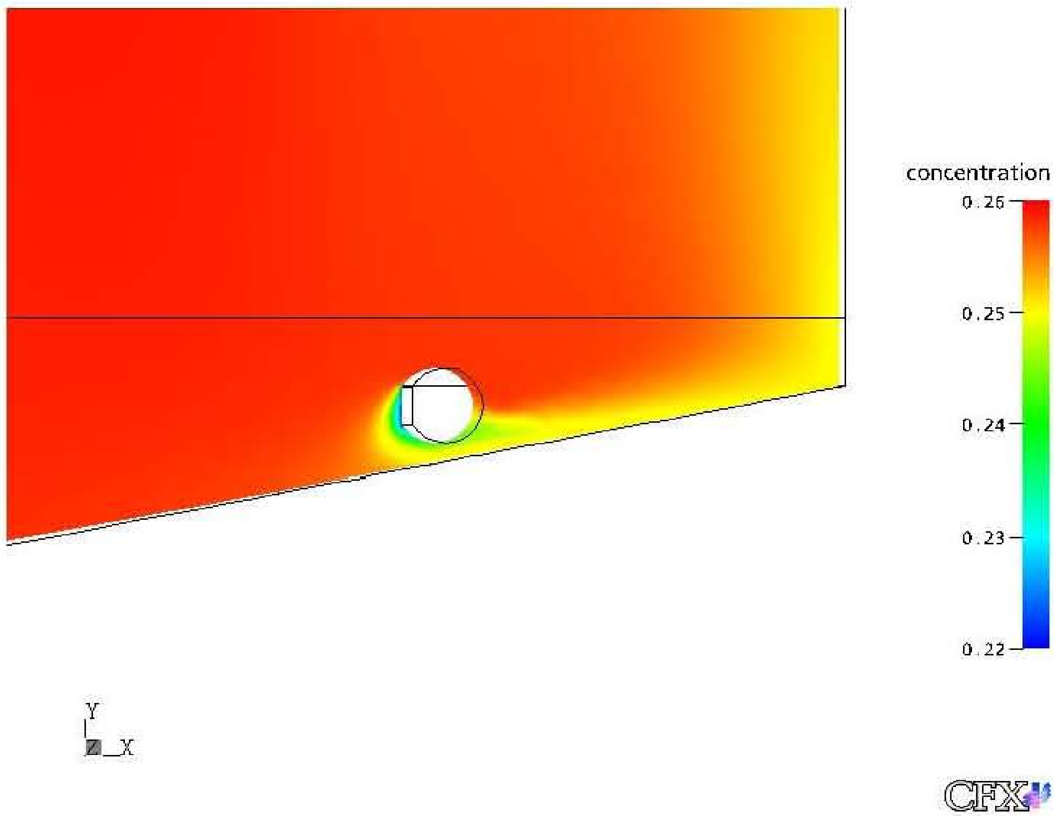

Figure 6.11 Close up juice brix plot of the flow around the inlet from Figure 6.10

Figure 6.10 shows that a majority of the juice inside the vessel is at a relatively high brix, comparable to the outlet, with only the juice in the immediate vicinity of the juice inlet pipe at relatively low brix. Figure 6.11 shows the large gradients in juice brix in the vicinity of the juice inlet pipe caused by the mixing action occurring in this region. Figure 6.12 is a vector plot on a horizontal plane that passes through the centre of the juice inlet pipe. Figure 6.13 is a juice brix plot on the same horizontal plane as Figure 6.12.

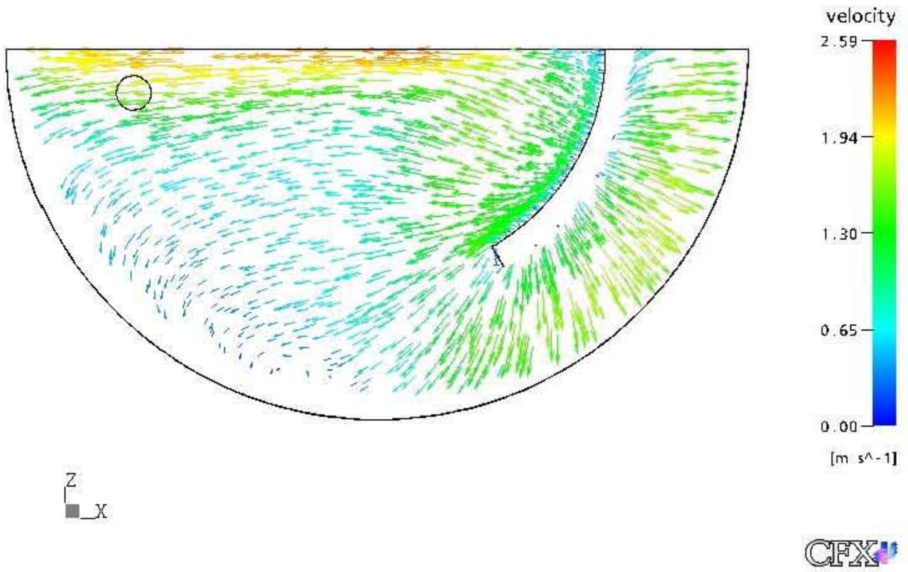

Figure 6.12 Vector plot on a horizontal plane through the centre of the juice inlet pipe for the Farleigh #2 vessel

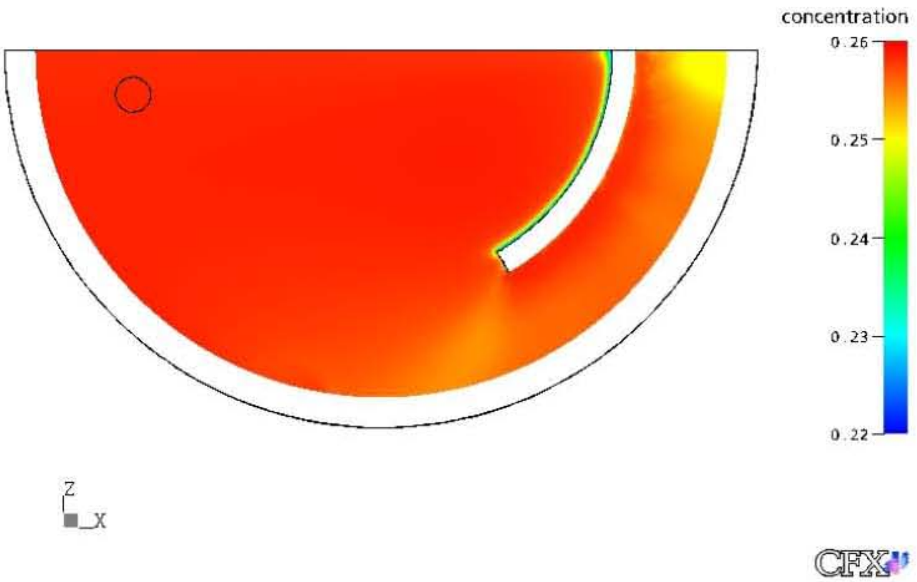

Figure 6.13 Juice brix plot on a horizontal plane through the centre on the juice inlet pipe for the Farleigh #2 vessel

Figure 6.12 shows that juice flows away from in the inlet predominantly in two directions. This behaviour causes the relatively high brix juice, after mixing, from the region around the inlet pipe being transported and mixed throughout the remainder of the vessel. Figure 6.13 shows the localised area of relatively low brix juice around the juice inlet pipe and is further evidence of the mixing action occurring inside the vessel.

The total quantity of juice flowing into the vessel is 380 $t{\cdot}h^{-1}$ with 329 $t{\cdot}h^{-1}$ flowing out and 51 $t{\cdot}h^{-1}$ of water is evaporated and flows out of the vessel as vapour. The total amount of juice flowing down in the calandria is approximately 33 000 $t{\cdot}h^{-1}$ or 87 times the amount of juice flowing into the vessel. Similar to observations from the Proserpine #4 predictions, the amount of internal fluid recirculation causes energy wastage and helps to explain why the vessel is well mixed.

6.4 Deficiencies in the existing vessel design

Analyses of the results from the Proserpine #4 and the Farleigh #2 vessel, although different in size, show similar deficiencies in flow behaviour. The juice flowing from the inlet rapidly mixes with juice flowing down through the calandria and then short circuits almost directly towards the outlet, with very little mixing with the juice in the remainder of the vessel. This in turn causes large quantities of juice to re-circulate inside the vessel consequently wasting energy and causing all of the juice inside the vessel to be of a high concentration.

The largest gradients in juice brix occur in the immediate vicinity of the juice inlet and the motion of the juice flowing from the inlet transports the relatively high brix juice throughout the remainder of the vessel. The end result of this mixing action is that a majority of the heating tubes in both vessels are in contact with juice that is at a brix that is very close to the juice brix at the outlet of the vessel. The high brix juice contacting the heating tubes causes a reduction in the driving force for heat transfer. Therefore, the vessel relies on the recirculation of juice through the heating tubes to achieve the evaporative duties required.

The flow behaviour observed in the Proserpine #4 and the Farleigh #2 vessels suggests that future improvements in the design of evaporator vessels should be focussed on separating the juice flow and forcing it to flow from the inlet, through the calandria and towards the outlet. This would reduce the mixing action observed in the existing vessels and encourage the relatively low brix juice flowing into the vessel to contact the heating tubes directly, without being mixed with higher brix material that has already passed through the calandria.

Both the Proserpine #4 and the Farleigh #2 vessels had significant quantities of juice being re-circulated inside the vessel. The large quantities of energy required to move the re-circulating fluid is extremely wasteful and could better be utilised in moving the juice from the inlet directly towards the outlet.

It is possible to achieve improvements in heat transfer with technologies such as plate-type heat exchangers, falling-film type evaporators and multiple vessels in series on any given effect. However, all of these technologies are cost prohibitive in the sugar processing industry and a more cost effective solution is sought after in this investigation. Modifications to existing vessels and a novel linear type evaporator design have been considered as part of this investigation in an attempt to achieve some of the benefits without being cost prohibitive.

6.4.1 Modifications to the existing design

Initial design modifications considered for the two evaporator vessels used in this study were limited to modifications and retrofit alterations. This was done to minimise the cost of such changes and the modifications are therefore more likely to be implemented by the industry. Only modifications to the Farleigh #2 vessel were modelled, as is was considered to be the most likely to require modifications because it is the oldest vessel.

6.4.2 Modifications considered

Modifications considered for the Farleigh #2 vessel are as follows:

- the inclusion of a large central downtake,
- the inclusion of a number of smaller downtakes,
- the juice inlet system was extended so that a full ring manifold was formed on the inside of the vessel, and
- the vessel was fitted with a single, central juice outlet pipe connected to the bottom of the central downtake.

Since the vessel presently contains no downtakes of any sort this modification was included as a means of assisting with the establishment of a defined flow path for the boiling juice. The disadvantage is that some of the heating tubes were removed and the heating surface area of the vessel was therefore reduced. This was expected to be counteracted by an improvement in heat transfer performance. The smaller downtakes were located on two radial positions, situated away from the juice inlet. This was an attempt to separate the high brix juice flowing down the downtakes from the low brix juice flowing in through the inlet.

All of the modifications were applied to the vessel and a single CFD model run of the new geometry was completed. The combined effect of each modification was believed to be the most likely means of achieving the designed improvement in circulation and heat transfer performance. This approach saved time by reducing the number of required simulations but prevented the quantification of the expected improvement from each modification when applied individually.

Figure 6.14, Figure 6.15 and Figure 6.16 show the details of the geometrical modifications considered for the Farleigh #2 vessel, all of the operating conditions remained the same.

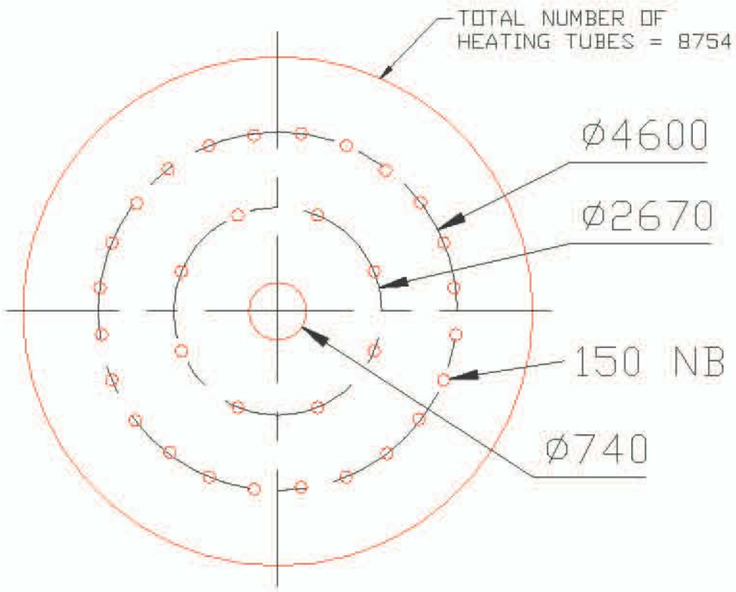

Figure 6.14 Top view of the modified calandria layout for the Farleigh #2 vessel

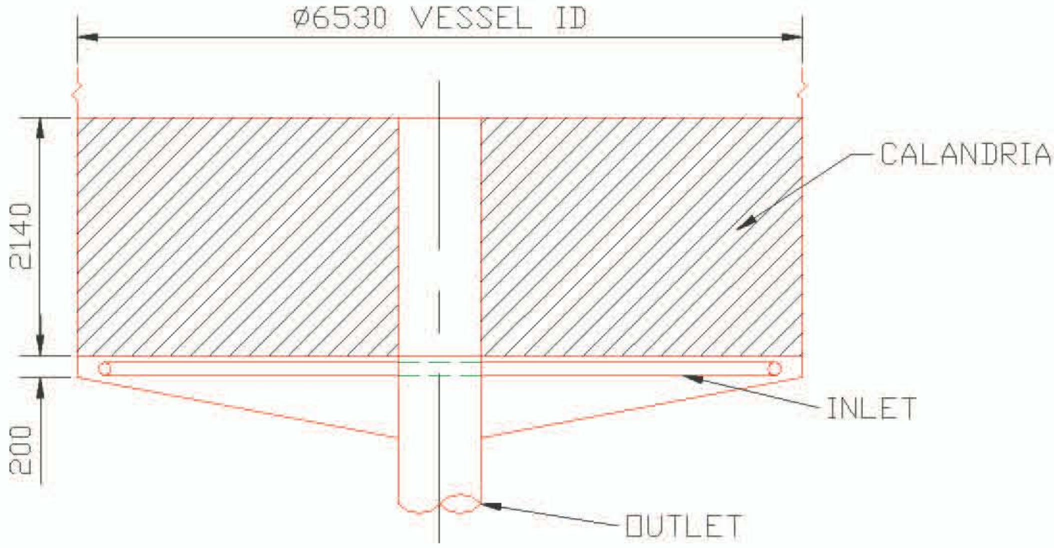

Figure 6.15 Side view of the modified juice inlet and outlet system for the Farleigh #2 vessel

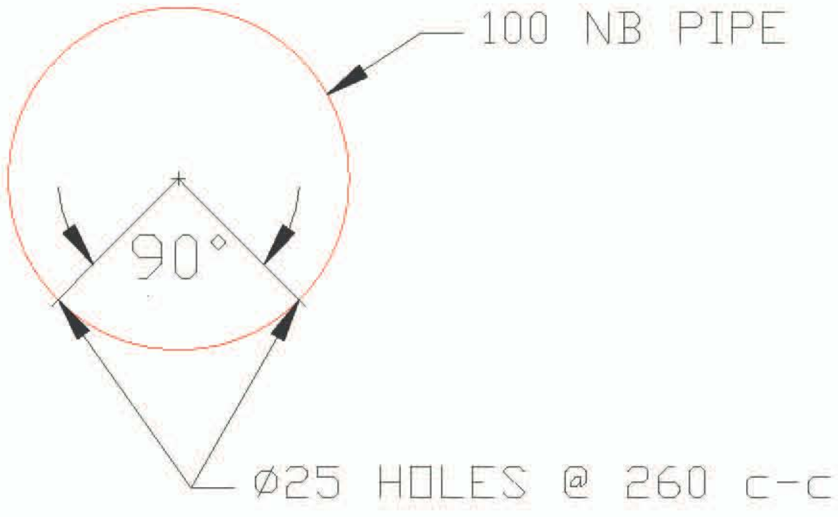

Figure 6.16 Details of the holes in the modified juice inlet manifold for the Farleigh #2 vessel

The purpose of all the modifications applied to the Farleigh #2 vessel was to aid juice circulation through the calandria of the vessel and to separate the juice flows at the inlet and outlet of the vessel. The juice inlet was changed to a fully circumferential ring manifold and was shifted towards the outer shell of the vessel. When combined with the central juice outlet, the predominant juice flow path is radially from the outer circumference of the vessel towards the centre of the vessel. If pure radial flow is achieved then the lowest brix juice introduced at the outer circumference of the vessel will be exposed to the largest possible heating surface area.

With the juice outlet connected to the bottom of the large central downtake there is more distance between the juice inlet and juice outlet, with the calandria in between. The most likely juice flow path is then from the juice inlet, up through the calandria, across the top of the tube-plate and down the large central downtake to the outlet. The expected result is a small amount of juice existing above the top tube-plate will flow back down the small downtakes, and mix with the low brix juice flowing from the inlet, but this amount is significantly reduced compared to the existing design. If the juice is allowed to drain from the region above the top tube-plate then the boiling action inside the heating tubes is not suppressed by the extra head above the top tube-plate.

6.5 Modified Farleigh #2

6.5.1 CFD model details

The geometry of the modified Farleigh #2 vessels displays 1/8 symmetry and was modelled using a 45° wedge and two planes of symmetry. A mesh containing 246901 nodes was applied to the geometry. All remaining details and boundary conditions were kept the same as the previous model runs for the Farleigh #2 vessel. The mesh density in the region around the juice inlet and inside the downtakes was set finer than the remainder of the vessel for the same reasons as previously discussed (Figure 6.17).

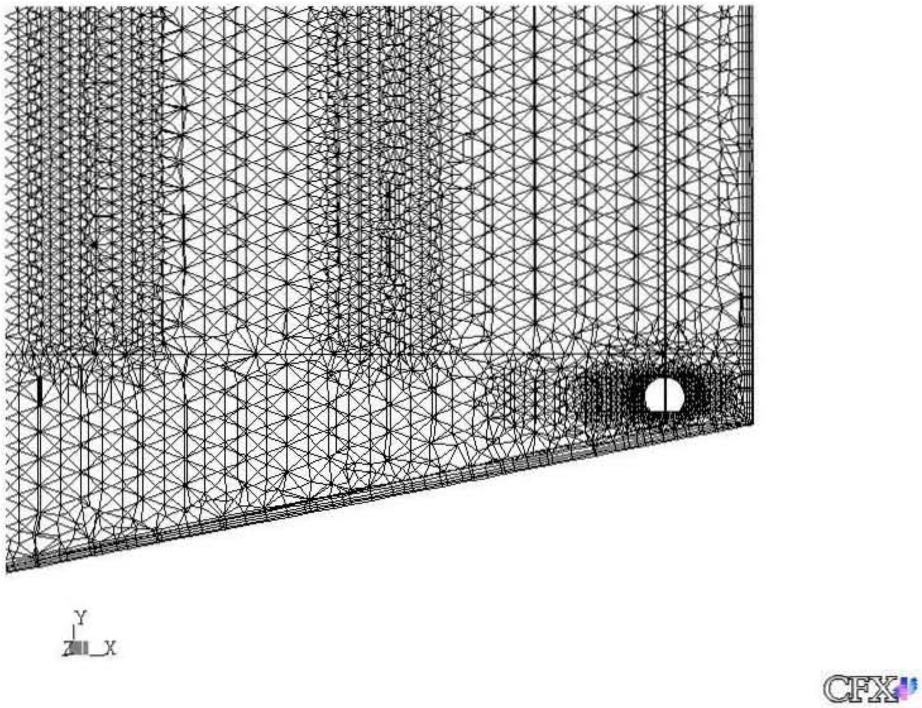

Figure 6.17 Mesh applied to the modified Farleigh #2 geometry

6.5.2 Circulation patterns

The predicted flow behaviour inside the modified Farleigh #2 vessel has improved by a small amount but still displays similar mixing behaviour as was previously predicted with the existing geometry. Figure 6.18 shows that the predicted concentration throughout the majority of the vessel is relatively high when compared to the juice brix at the outlet of the vessel. This behaviour suggests that there is still a lot of mixing occurring inside the vessel in spite of the modifications.

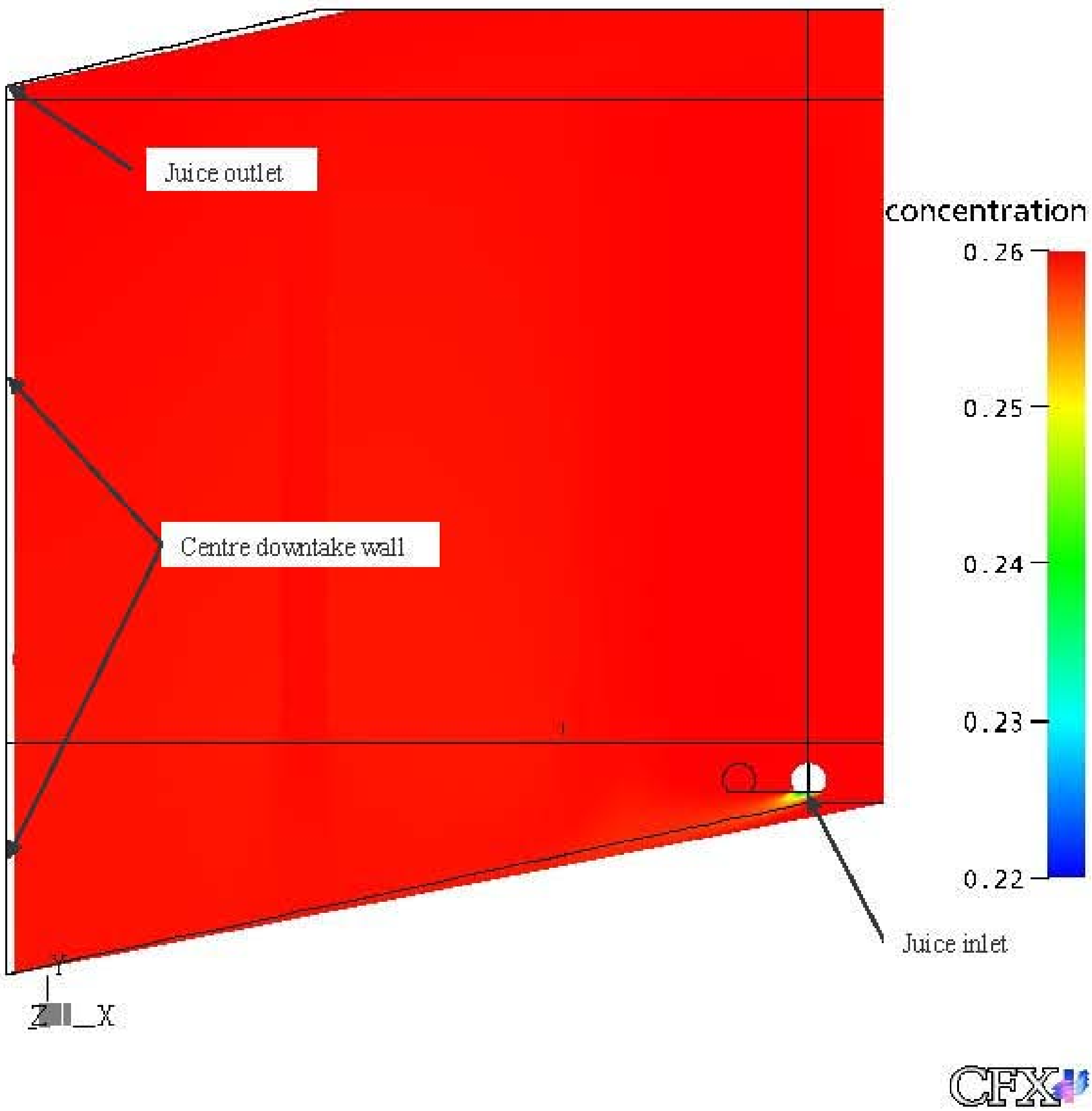

Figure 6.18 Juice brix plot on a vertical plane through the centre of the wedge for the modified Farleigh #2 geometry

Figure 6.19 shows that there is some improvement in the flow path within the vessel with a significant portion of the downward flow occurring through the smaller downtakes. A downward flow is predicted in the heating tubes adjacent to the external shell of the vessel.

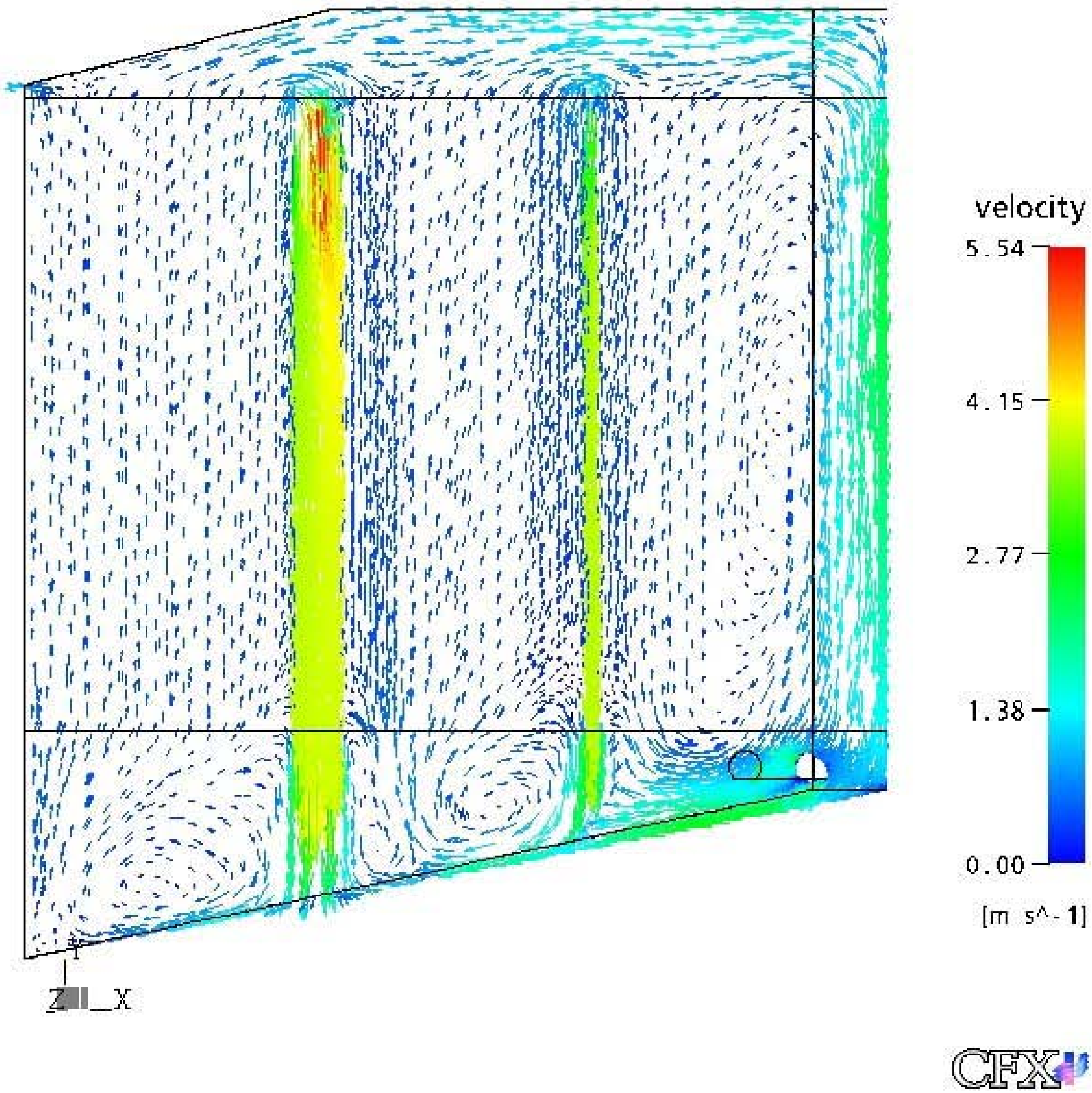

Figure 6.19 Vector plot on a vertical plane through the centre of the wedge for the modified Farleigh #2 geometry

The downward flow predicted in the heating tubes against the exterior shell of the vessel with the modified geometry is significantly smaller than the downward flow predicted through the heating tubes inside the existing Farleigh #2 vessel. This suggests that the modifications applied to the geometry have succeeded in reducing but not eliminating the downward flow in the heating tubes. This is likely to be rectified by increasing the number of smaller downtakes distributed around the calandria.

Figure 6.20 shows that the juice brix below the calandria is relatively high when compared to the juice brix at the outlet. This suggests that there is still significant amounts of mixing occurring inside the vessel and that significant quantities of high brix juice is flowing from the region above the top tube-plate to mix with the low brix juice flowing in through the juice inlet manifold.

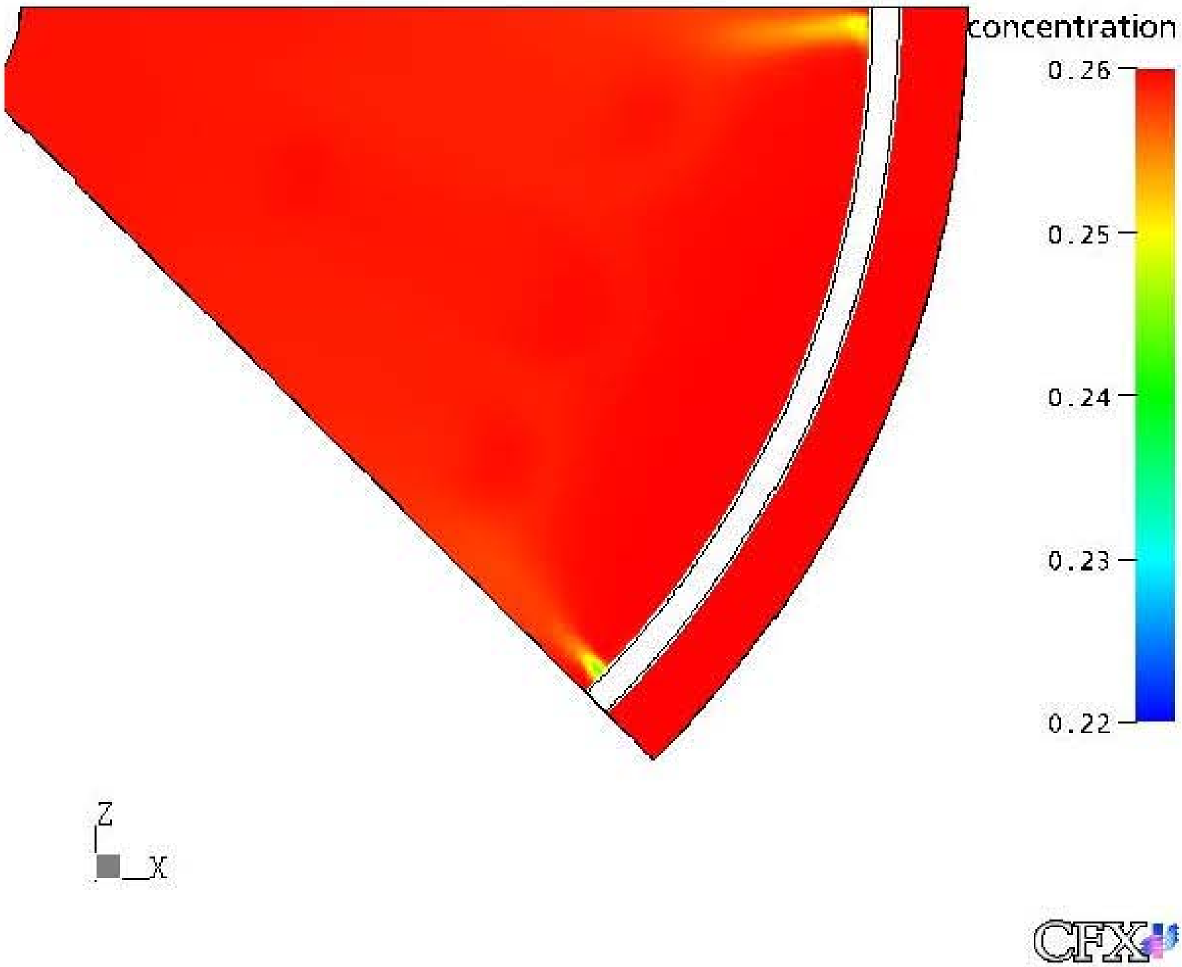

Figure 6.20 Juice brix plot on a horizontal plane through the centre of the juice inlet manifold for the modified Farleigh #2 geometry

Figure 6.21 shows that the juice flowing down the heating tubes on the outer shell of the vessel is turning and flowing across the juice inlet manifold. This is likely to be the major cause of the mixing action occurring inside this vessel.

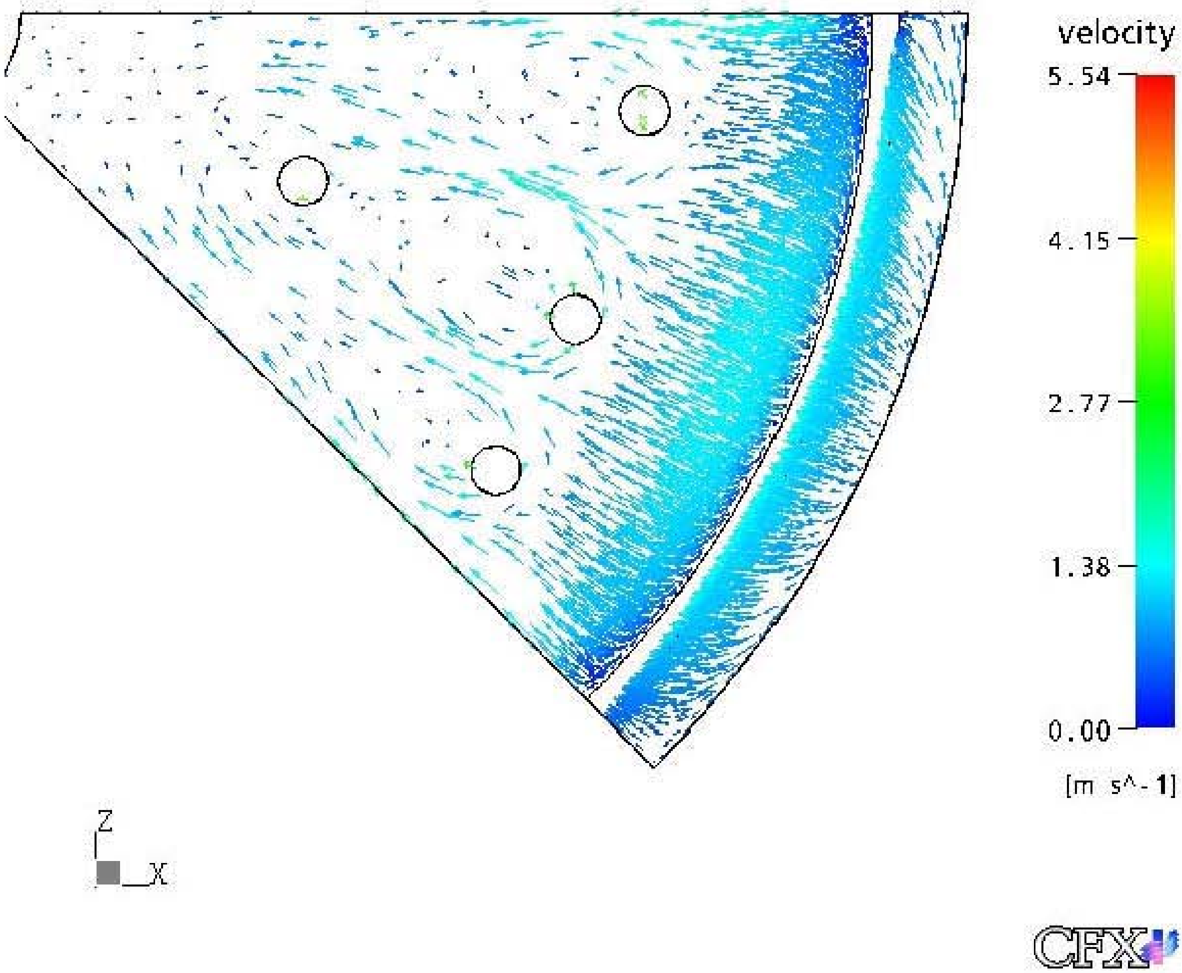

Figure 6.21 Vector plot on a horizontal plane through the centre of the juice inlet manifold for the modified Farleigh #2 geometry

Figure 6.21 shows that there is a region of almost stagnant juice flow in the centre of the vessel below the calandria. This stagnant region is not likely to be causing any significant reduction in heat transfer performance but should be avoided because it is additional fluid volume within the vessel that is not needed and increases the capital cost of construction unnecessarily.

Figure 6.21 shows that the predicted juice flow path in the horizontal plane is predominantly in the radial direction. This suggests that the modifications applied to the Farleigh #2 vessel have improved the predicted flow path a little but there are still further improvements to be realised.

The total mass flow quantities flowing into and out of the vessel are the same as the Farleigh #2 (380 $t \cdot h^{-1}$ in, 329 $t \cdot h^{-1}$ out and 51 $t \cdot h^{-1}$ of water is evaporated). The total amount of juice flowing down in the calandria is approximately 29 000 $t \cdot h^{-1}$ or 75 times the amount of juice flowing into the vessel. When compared to the 33 000 $t \cdot h^{-1}$ in the existing geometry, the modifications applied have reduced the amount of re-circulating juice. However, this is only a small improvement and there are still large quantities of energy wasted in re-circulating juice inside the vessel.

These results indicate that the circulation pattern inside the Farleigh #2 vessel can be improved by modifying the inlet and outlet designs and fitting downtakes to the calandria. Although some separation of the juice inlet and outlet flows has been achieved, the improvements are small it is likely that further modifications will be able to provide bigger improvements. The flow behaviour in the modified vessel is closer to plug flow but there is still a very large quantity of juice being re-circulated around inside the vessel. It is unlikely that this wasted energy will be able to be eliminated simply by modifying the current vessel design. A novel design approach may be required to achieve this.

6.5.3 Heat transfer performance

To quantify the benefits achieved by the modified geometry, the heat transfer performance of the vessel was predicted. For comparison purposes, performance is displayed here as the heat transfer coefficient (HTC). Previous discussions on predicted heat transfer performance have used only the total quantity of heat flowing through the calandria. In this case the HTC is used because the inclusion of the downtakes into the modified Farleigh #2 geometry has reduced the overall heating surface are of the vessel. Therefore, the HTC is used for comparison purposes since it provides common grounds for comparison.

For the operating conditions detailed for test No. 1 on the Farleigh #2 vessel, the predicted HTC was 530.3 $W \cdot m^{-2} \cdot K^{-1}$ and the for the modified geometry was 532.9 $W \cdot m^{-2} \cdot K^{-1}$. This shows only a very small improvement in HTC (0.5%).

If the radial flow behaviour can be maintained and the downward juice flow in the outer heating tubes adjacent to the shell of the vessel can be eliminated then the mixing action occurring inside the vessel is likely to be significantly reduced. As a consequence the predicted juice brix distribution and the heat transfer performance of the vessel should improve.

The results of the investigation involving retro-fit modifications to date have shown potential to deliver improvements in vessel performance if further investigations along these lines are completed. The principles of attempting to achieve radial type flow and minimal mixing within the vessel should be maintained if this research path is followed. Further investigation involving low cost modification to the existing design of vessels is considered to be outside the scope of this investigation. Instead, radical changes in vessel design will be considered in order to achieve the same principles of minimal mixing within the vessel. Although these radical changes involve the construction of completely new vessels, the additional cost is believed to be justified by the potentially very large improvement in vessel performance.

6.6 Novel evaporator design

In order to achieve a juice flow pattern that separates the juice flows at inlet and at outlet and to reduce the amount of juice re-circulating inside the vessel, a linear system of cells operating in series was devised. Without the limitations of maintaining a cylindrical vessel, a vessel containing a number of square shaped cells was devised. The idea was for the juice to pass upwards through the heating tubes once then down a downtake to the inlet of the next cell.

6.6.1 Details of the design

The proposed new linear system consists of a number of cells operating in series with the geometry of each cell being identical. Figure 6.22 is a side view of one cell and shows the details of the geometry.

Each cell is 2.0 m wide and contains 589 heating tubes, resulting in a heating surface area of 167.6 m^2. There are no downtakes included in the calandria section.

The design allows flexibility for any number of cells to be joined in series to achieve the desired total heating surface area. This also provides a simple and easy means of making a small increase to the total heating surface area capacity of the vessel. The width of the cells was limited to 2.0 m for the purposes of this study but is an area for further research if this design is to be investigated further.

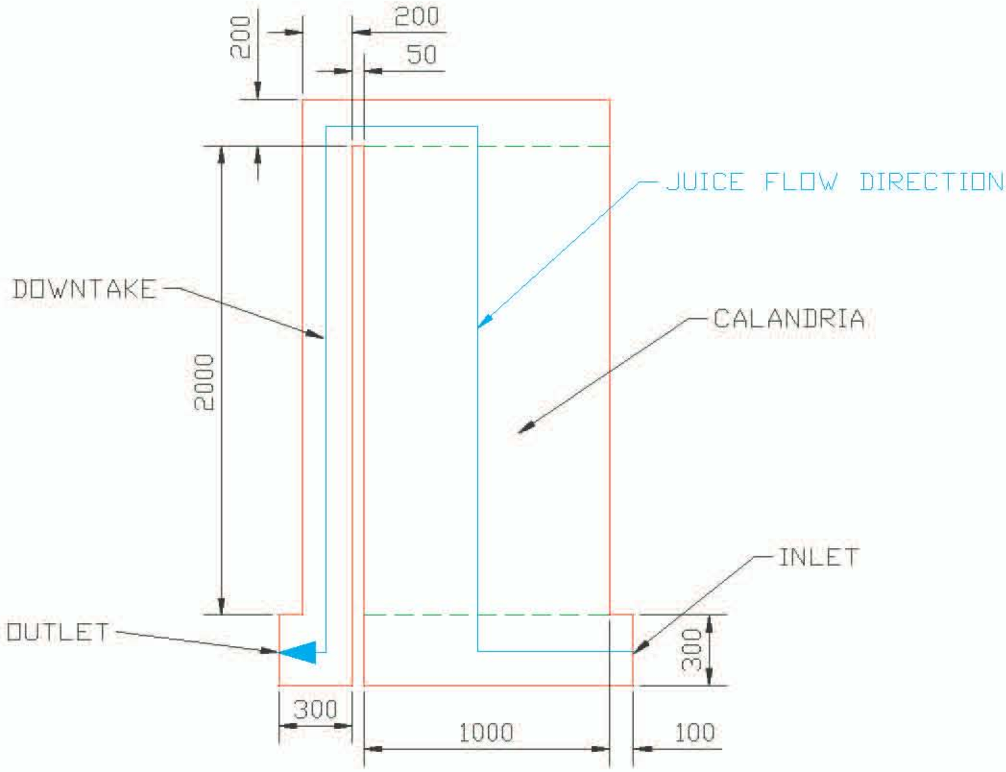

Figure 6.22 Details of each cell in the linear design

Any number of cells can be joined together to operate any one effect and any number of effects can be joined together to operate as a complete evaporator station. In this case three cells have been placed on the first three effects and four cells have been placed on the fourth and final effect. The total number of cells considered in this case is 13.

6.6.2 CFD model details

The geometry of the linear vessels was modelled in 2-D since it was assumed that adequate flow distribution at the juice inlet will be achieved. Similar flow distribution has been demonstrated in other parts of the sugar factory, including vacuum filters, and it is assumed that the same can be achieved in the evaporator station. It is recognised that 3-D flows may develop inside the vessel but the size of the model to be considered is limited by the computing resources available. It is unlikely that the edge effects of the side wall and other influences will cause 3-D flows to dominate the flow field.

A mesh containing 152251 nodes was applied to the geometry of one cell. Due to the 2-D nature of the geometry the mesh density everywhere in the cell was increased significantly without exceeding the memory limitations of the available hardware. However, the total run time involved in simulating the entire linear evaporator was significantly longer than for the circular shaped vessels. Each cell is modelled individually using the same mesh and the outlet conditions from the previous cell are set as the input conditions for the subsequent cell. Running the models of each cell in series increases the total run time that ultimately dictated the final size of the mesh applied to each cell of the linear evaporator. Figure 6.23 shows a close up of the mesh applied to the inlet of the novel evaporator design.

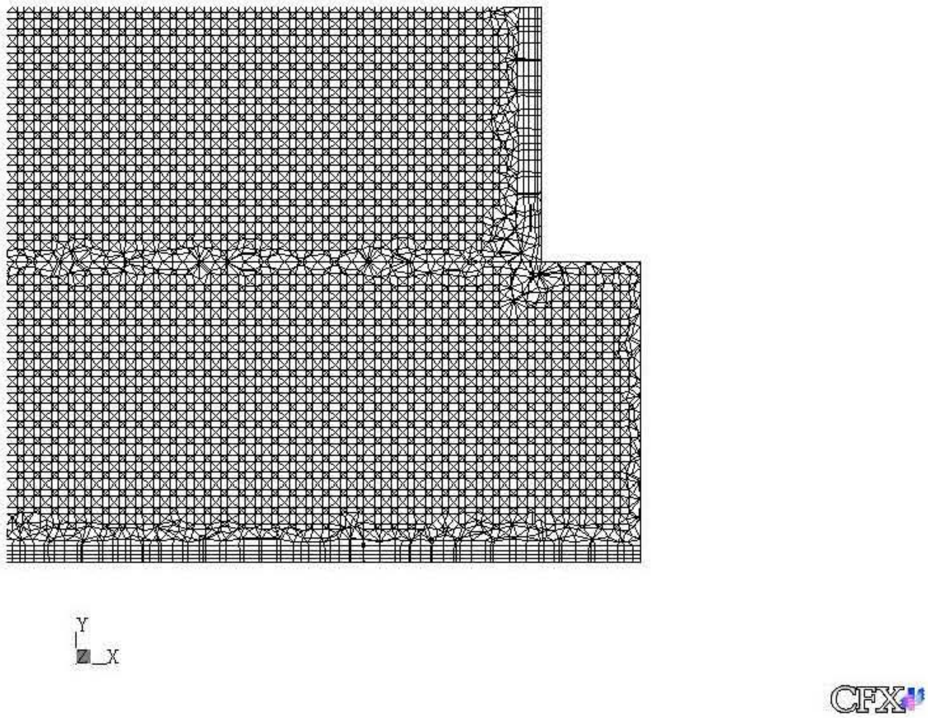

Figure 6.23 Mesh applied to one cell of the linear evaporator geometry

Each cell was modelled individually with the operating conditions at the outlet of the first cell being applied as the inlet conditions to the second cell and so on. A second effect was modelled using three cells in series with initial operating conditions being similar to the average conditions measured during the six tests conducted on the Farleigh #2 vessel. This provided a suitable means for comparing the performance of the two designs. A final effect was modelled using four cells in series with the initial operating conditions being similar to the average conditions measured during the four tests conducted on the Proserpine #4 vessel. This also provided a suitable means for comparison.

6.6.3 Circulation patterns

The predicted juice flow patterns inside each cell of the linear evaporator design show that there is no downward flow of juice through the heating tubes and there is a steady increase in juice brix as the juice flows upwards through the tubes. Figure 6.24 shows the typically predicted juice flow and Figure 6.25 shows the predicted velocity profile inside the first cell of the second effect. This fluid behaviour is typical of what is predicted inside each cell of the linear evaporator. The length of the vectors in this plot is constant, for clarity, and the colours indicate magnitude.

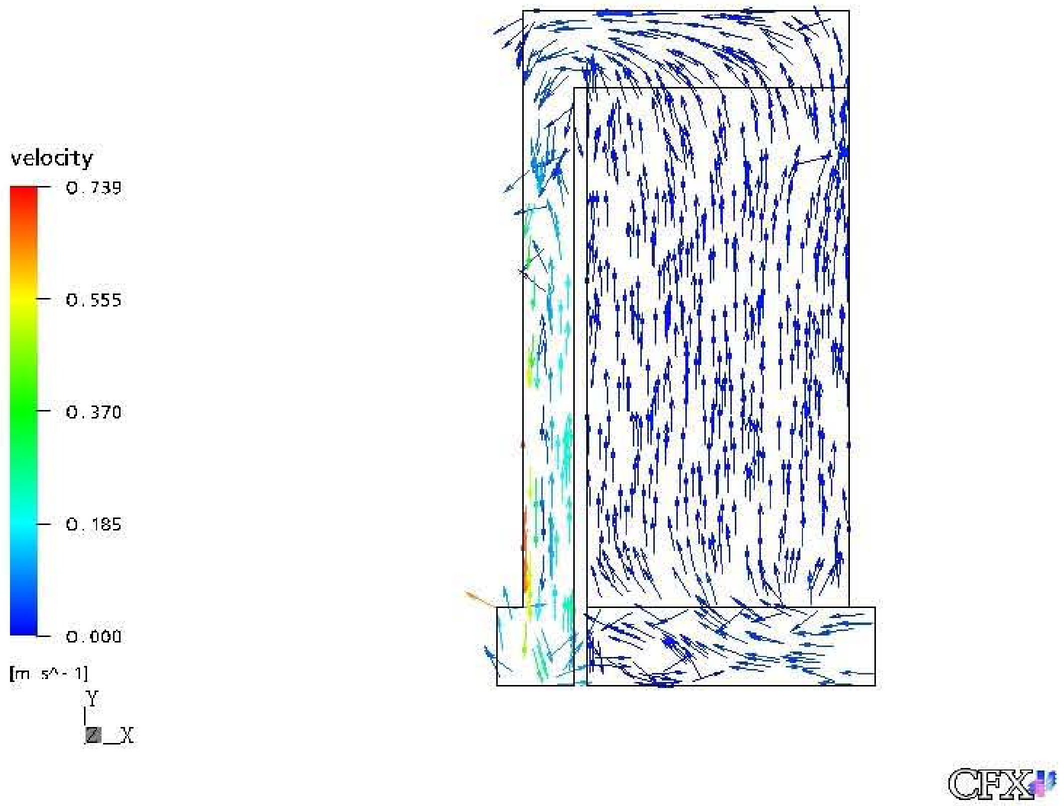

Figure 6.24 Vector plot on a vertical plane inside one cell of the linear evaporator

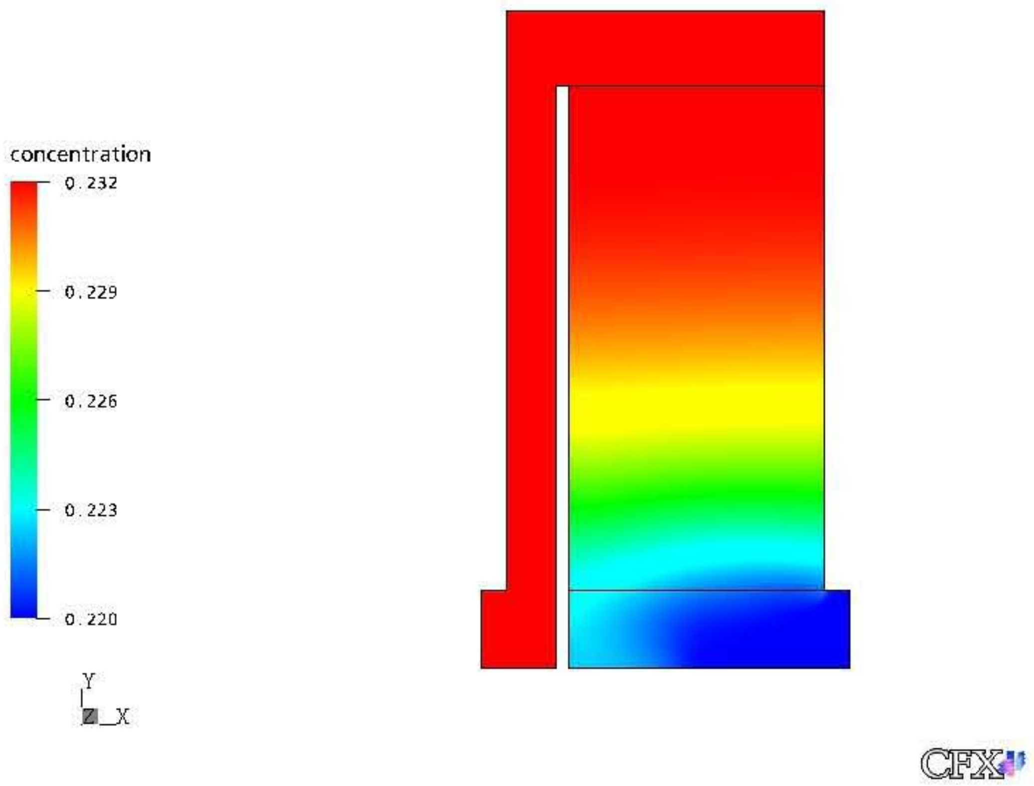

Figure 6.25 Juice brix plot on a vertical plane inside one cell of the linear evaporator

When compared to the predicted fluid flow behaviour inside the existing vessel geometries, the cells of the linear evaporator show significantly less mixing occurring in the region under the calandria, thus exposing the heating tubes to juice that is at a brix which is very similar to the juice brix at the inlet to the cell. By placing a number of cells in series the juice is guaranteed to flow through the calandria at least three times without mixing. In the case of the modified Farleigh #2 geometry the juice is guaranteed to pass through the calandria only once and for existing geometries it is possible for the juice to flow from the inlet to the outlet without passing through the calandria.

The re-circulation suffered by the circular design of vessels has been eliminated with this design and the consequent wasted energy in moving large quantities of fluid around inside the vessel has been avoided. The CFD model predictions show that the linear evaporator design is able to achieve separation of the juice flows at inlet and at outlet. The juice passes through the calandria of each cell only once but does so at juice conditions that increase the driving force for heat transfer.

Figure 6.26 and Figure 6.27 show the gradual increase in brix as the juice passes through each cell. This flow behaviour comes as a result of the limited amount of juice mixing that occurs in the region under the calandria.

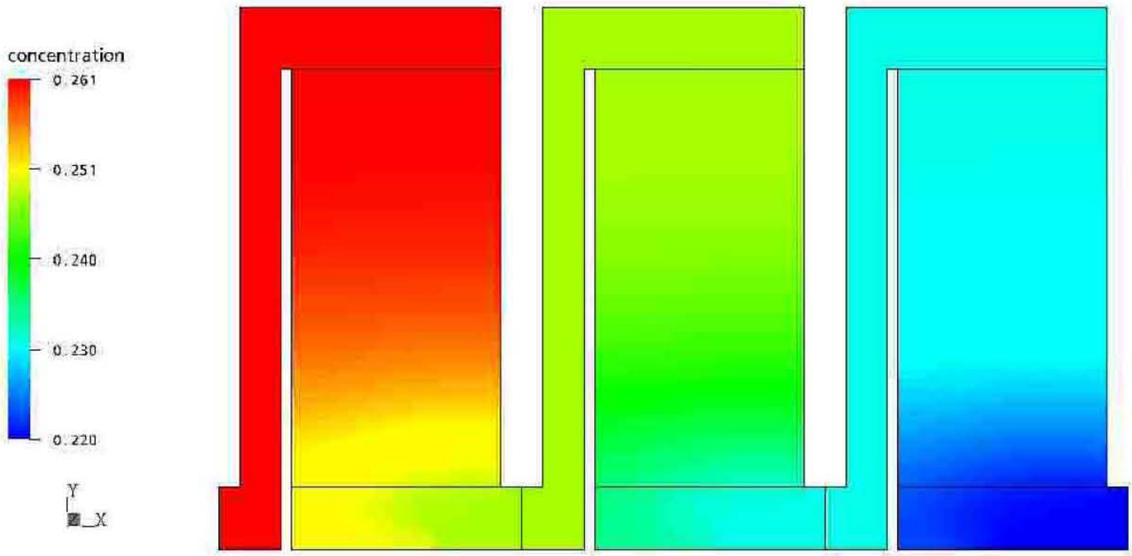

Figure 6.26 Juice brix plot on a vertical plane inside the three second effect cells of the linear evaporator

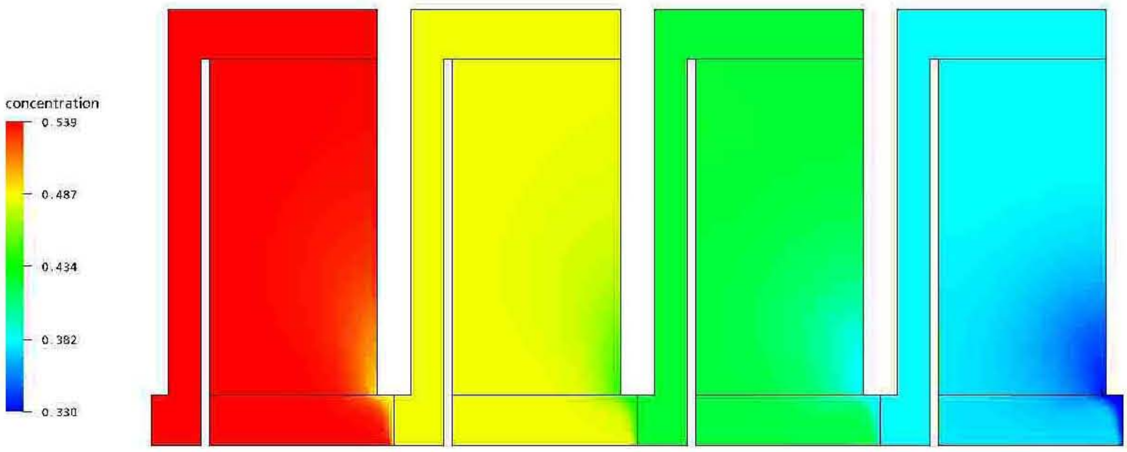

Figure 6.27 Juice brix plot on a vertical plane inside the four fourth effect cells of the linear evaporator

6.6.4 Heat transfer performance

Due to the long run times involved in the prediction, the test conditions for test No 1. of the Farleigh #2 and the Proserpine #4 respectively were used to define the boundary conditions of the model when using the linear geometry. This provides some common basis for comparison and demonstrates the difference in heat transfer performance of the linear design.

The predicted HTC for the three cells of the linear evaporator that perform the duties of the second effect were 2861 $W \cdot m^{-2} \cdot K^{-1}$, 2272 $W \cdot m^{-2} \cdot K^{-1}$ and 2294 $W \cdot m^{-2} \cdot K^{-1}$ respectively with an average of 2476 $W \cdot m^{-2} \cdot K^{-1}$. The average HTC predicted for the six tests conditions modelled on the Farleigh #2 vessel was 1829 $W \cdot m^{-2} \cdot K^{-1}$. This shows that the linear concept has a predicted 35.4% improvement in heat transfer performance over the existing Farleigh #2 evaporator design.

The predicted HTC for the four cells of the linear evaporator that perform the duties of the fourth effect were 580.4 $W \cdot m^{-2} \cdot K^{-1}$, 510.3 $W \cdot m^{-2} \cdot K^{-1}$, 495.4 $W \cdot m^{-2} \cdot K^{-1}$ and 404.0 $W \cdot m^{-2} \cdot K^{-1}$ respectively with an average of 497.5 $W \cdot m^{-2} \cdot K^{-1}$. The average HTC predicted for the four tests conditions modelled on the Proserpine #4 vessel was 372.1 $W \cdot m^{-2} \cdot K^{-1}$. This shows that the linear concept has a predicted 33.7% improvement in heat transfer performance over the existing Proserpine #4 evaporator design.

Other practical advantages associated with the linear design such as cost of manufacture, ease of capacity expansion and operating costs have not been considered as part of this investigation. If the novel design presented here is to be developed further then these factors need to be considered because it is possible that the additional pumping costs, etc., may make the new design impractical.

6.7 Summary of model predictions

The modelling results presented in this chapter predict that small improvements in circulation patterns and heat transfer performance can be achieved through the application of some minor modifications to the existing design configurations of evaporator vessels. While the addition of a circumferential inlet, central outlet and downtakes to the calandria of a circular vessel improves heat transfer performance it must be considered that the total heating surface area of the vessel is reduced slightly. This disadvantage must be considered against the performance improvement and the relatively small cost and risk associated with these modifications. The results predict that the linear design is capable of achieving larger improvements in performance, but the cost and risk of the design have not been considered.

A reduction in the amount of re-circulation occurring inside the vessels is important because it reduces the chance of mixing and reduces the amount of energy wasted in moving that large quantity of fluid. The modifications applied to the Farleigh #2 vessel are able to provide a small improvement in the circulation patterns by providing a more radial flow path for the juice. However, the novel linear design is capable of almost eliminating any mixing of juice prior to passing through the calandria and any energy wasted in re-circulation. The separation of the juice flows at inlet and at outlet results in more favourable juice conditions inside the heating tubes.

The scope of this investigation have not included all of the factors associated with the development of an improved evaporate design. However, the current direction of research has shown some potential and the CFD modelling tools developed as part of this investigation have also shown potential.

Future investigations into design improvements should consider the following points:

- The overall cost of modification / installation;
- The cost and effort required for small incremental increases in overall factory capacity;
- Changes to critical dimensions of circular vessels including the tube length and vessel diameter, the number and placement of downtakes in the calandria and the shape of the bottom of the vessel; and
- Changes to critical dimensions of linear vessels including the tube length, vessel width, the size and shape of the juice region under the calandria and the number of cells placed in series.

7. Summary, conclusions and recommendations

As a result of this investigation into the development of a more energy efficient Roberts evaporator a number of conclusions can be drawn. This study has included a broad scope containing factory experiments, CFD model development, CFD model validation and CFD model application.

7.1 Factory experiments

Prior to the commencement of this investigation the literature did not contain any data gathered from factory vessels that was suitable for comparison with the predictions obtained from a CFD model. Such data is essential for the development of a CFD model that is capable of producing accurate predictions. The methodology developed as part of this investigation produces accurate data in the juice region below the calandria. However, due to the discovery that a majority of the juice brix gradients occur immediately adjacent to the inlet, the data gathered to date is within a smaller band than what would be ideal. All of the juice brix measurements are very close in magnitude to the juice brix at the outlet of the vessel, rather than being evenly spaced between the juice brix at inlet to outlet.

Only a very small number of data points were located inside the heating tubes and none were located in the region above the top tube-plate. The multi-phase nature of the fluid flows in both of these regions justifies the gathering of further data from there. The calandria is a critical part of the vessel and dominates the fluid flow behaviour in the remainder of the vessel. Due to the complex nature of the calandria and the assumptions involved in modelling, factory data gathered from within the calandria and from above the top tube-plate would allow the determination of the accuracy of model prediction in this area.

The conclusion drawn from the factory experiments conducted as part of this investigation is that suitable data for comparison with CFD model predictions is now available for future developmental work. While there are some deficiencies associated with the data it is of suitable accuracy and quantity to be useful.

As a result of the factory experiments conducted as part of this investigation it is recommended that the same experimental procedure be used to take further measurements in the juice region immediately adjacent to the juice inlet, inside the heating tubes and in the region above the top tube-plate.

A CFD model should predict all of the physics associated with the fluid flow but the accuracy of any evaluations performed on the model predictions is dependant on the ability to perform precise experimental measurements. The experimental data and the CFD model predictions obtained from this investigation indicate that there is a large amount of flow behaviour detail that remains unknown. It is recommended that future studies consider conducting lab scale experiments to complement the factory scale experiments. The lab scale experiments should focus on visualisation of the juice flow in the entire vessel. This understanding of juice flow behaviour will aid the in the refinement of the CFD model.

7.2 CFD model development

The CFD model has shown to be computationally intensive due to the large number of finite volumes required to represent the geometry of the vessel. In this study complete mesh independence was not achieved due to the memory hardware limitations of the computer used to solve the equations. This is one of the limitations of the results displayed herein, and should be considered prior to the commencement of any follow on work.

The simplifying assumptions required to model the calandria section are critical to the model's ability to produce accurate predictions of the fluid flow inside an evaporator vessel. The results in Chapter 6 show that the fluid flow in the calandria section, in particular the downtakes, has an over riding influence on the fluid flow in the remainder of the vessel. The application of large body forces in the horizontal plane to simulate the vertical walls of the heating tubes proved successful in this case, but contributed to the large run times required to achieve convergence.

The inclusion of the vapour phase at juice inlet is a significant improvement that would improve the accuracy of predictions. It is recommended that future investigations include modelling of the effect of the vapour phase at juice inlet, provided the computing resources are available to handle the added complexity.

The Rhosenow equation used in this study to predict the total heat flow through the calandria was designed for clean stainless steel heating surfaces transferring heat to clean water. This was applied to a case where heat is transferred from stainless steel heating surfaces with varying degrees of fouling to sugar solutions. While the application of the equation in this investigation was successful as an initial step, success was limited when the tubes were highly fouled. The form of the equation includes a number of empirical constants that can be determined from test rig experiments using fouled tubes and sugar solutions under controlled conditions. Another possible improvement is to apply a totally different form of equation.

The CFD model development work completed herein requires further development to improve accuracy but it can be concluded that the CFD model developed as a result of this investigation is capable of producing useful predictions of the fluid flow inside sugar mill evaporator vessels.

It is recommended that future studies examine the hardware requirements well prior to undertaking any development so that a suitable machine is available for modelling. The machine should contain enough physical memory so that the required number of finite volumes can be used and complete mesh independence can be achieved. The machine should also contain a CPU fast enough to provide convergence on a large mesh within a reasonable amount of time.

It is recommended that future model development focus on the restriction of fluid movement in the horizontal plane to include an improved expression for the prediction of the total heat flow through the calandria and make an allowance for the effect of scale growth on the heating tubes. The improvements to the expression could include refinements to the empirical constants within the current expression or a totally different expression. These improvements will significantly improve the accuracy of the model predictions.

7.3 CFD model application

Application of the model developed as part of this study demonstrated potential improvements in heat transfer, mixing and fluid circulation can be achieved by modifying vessel geometry. It is possible to achieve small improvements from retro-fit modification to existing vessels but the magnitude of the benefits achieved is limited. The inclusion of a circumferential juice inlet system, a central juice outlet and the inclusion of downtakes in the calandria produced a more radial flow inside the vessel which is closer to a plug flow than the current flow pattern. However, the vessel remains well mixed with substantial recirculation.

CFD model predictions show that the existing evaporator vessel design has significant deficiencies and it is concluded that the greatest improvement in the flow pattern was achieved by adopting a totally new concept in evaporator design. The system containing a large number of rectangular shaped calandrias and downtakes (cells) in series is a novel evaporator design (linear evaporator design). The CFD model predictions show a complete elimination of the juice mixing at the inlet and of re-circulation within the calandria. This reduces the average juice brix in the region below the calandria and in the calandria itself. As would be expected, the overall heat transfer performance improved in line with the improvements in fluid flow patterns.

The development of the linear evaporator design was achieved without practical consideration of what might be required to implement it. While the linear evaporator design shows significant improvement in the flow patterns and a predicted improvement in heat transfer performance of greater than 30%, the following factors are considered important if further development of the design is to be worthwhile:

- The cost of installation and operation,
- The capacity for incremental increases in capacity to be added,
- The capacity for a new type of vessel to be integrated into an existing factory with existing evaporator vessels, and
- The capacity for the vessel to be implemented into a system where large quantities of vapour are bled off, such as the case where a factory has a large co-generation capacity.

These conclusions have been drawn from the results of modelling done as part of this investigation. It must be recognised that the scope of potential geometry changes is significantly larger than was able to be included in this investigation and it is possible that other modifications may be able to produce greater improvements. One area in particular that has not been investigated is the length and diameter of the heating tubes inside the calandria.

As a result of the potential improvements in heat transfer performance that have been identified in this study, it is recommended that further investigations into retro-fit modifications be completed. These should include varying the length and diameter of the heating tubes. Any modifications actually installed in factory vessels should have a subsequent confirmation and quantification in the improvement in heat transfer.

The potential for significant improvement in the novel linear evaporator design should be further investigated with more CFD modelling and some pilot scale studies. The practical factors of implementing such a design should be considered at an early stage so as to provide some guidance on the actual running of a vessel. This will prevent large amounts of effort being invested into the modelling and development of the design if the concept is not practical in its application.

References

Abernethy, P. E., O. L. Crees, et al. (1991). Evaporator scale inhibition evaluation. Proceedings of the 13th conference of the Australian Society of Sugar Cane Technologists (ASSCT), Bundaberg, Queensland, Australia, Watson Ferguson and Company, Queensland, Australia.

Alfa-Laval (2001). Alfa-Laval Promotional Material.

Attard, R. G. (1991). Evaporator performance at Farleigh Mill. Proceedings of the 13th conference of the Australian Society of Sugar Cane Technologists (ASSCT), Bundaberg, Queensland, Australia, Watson Ferguson and Company, Queensland, Australia.

Batterham, R. J., J. A. Frew, et al. (1973). The use of boiling point rise for the control of pans. Proceedings of the 40th conference of the Queensland Society of Sugar Cane Technologists (QSSCT), Innisfail, Queensland, Australia, Watson Ferguson and Company, Queensland, Australia.

Broadfoot, R. and K. J. Dunn (2001). Demonstration and evaluation of energy efficient falling film evaporator technology in sugar mills. Mackay, Queensland, Australia, Sugar Research Institute (SRI): 44.

Bureau of Sugar Experiment Stations (BSES) (1992). Plant data 1991 season. Queensland, Australia, Bureau of Sugar Experiment Stations (BSES): 84.

Clift, R., W. R. Grace, et al. (1978). Bubbles, drops and particles, Academic Press, NY.

Crees, O. L. (1983). Scale inhibitors for sugar mill evaporators. Proceedings of the 5th conference of the Australian Society of Sugar Cane Technologists (ASSCT), Mackay, Queensland, Australia, Watson Ferguson and Company, Queensland, Australia.

DeViana, M. J., R. Broadfoot, et al. (1993). Performance evaluation of a plate evaporator. Proceedings of the 15th conference of the Australian Society of Sugar Cane Technologists (ASSCT), Cairns, Queensland, Australia, Watson Ferguson and Company, Queensland, Australia.

Doherty, W. O. S. (2000). Chemical cleaning of sugar mill evaporators. Proceedings of the 22nd conference of the Australian Society of Sugar Cane Technologists (ASSCT), Bundaberg, Queensland, Australia, Watson Ferguson and Company, Queensland, Australia.

Fulgosi, M., D. Lakehal, et al. (2003). "Direct numerical simulation of turbulence in a sheared air-water flow with a deformable interface." Journal of Fluid Mechanics(482): 319-345.

Grant, G., B. Morgenroth, et al. (2000). The Balcke-Duerr falling film plate evaporator - an innovative concept for evaporation in the cane industry. Proceedings of the 22nd conference of the Australian Society of Sugar Cane Technologists (ASSCT), Bundaberg, Queensland, Australia, Watson Ferguson and Company, Queensland, Australia.

Guo, S. Y., E. T. White, et al. (1983). Heat transfer coefficients for natural circulation evaporators. Proceedings of the 5th conference of the Australian Society of Sugar Cane Technologists (ASSCT), Mackay, Queensland, Australia, Watson Ferguson and Company, Queensland, Australia.

Henderson, C. S., B. J. Hellmuth, et al. (1981). The vertical louvre entrainment separator. Proceedings of the 3rd conference of the Australian Society of Sugar Cane

Technologists (ASSCT), Bundaberg, Queensland, Australia, Watson Ferguson and Company, Queensland, Australia.

Hong, Y., R. Sheikholeslami, et al. (2004). "Flow Boiling Heat Transfer of Water and Sugar Solutions in an Annulus." American Institute of Chemical Engineers Journal (AICHE) **50, No. 6**(June 2004): 1119-11128.

Incropera, F. P. and D. P. DeWitt (1996). Fundamentals of heat and mass transfer, fourth edition. Brisbane, Australia, John Wiley & Sons.

Ivin, P. C. and G. J. McGrath (1990). Acid cleaning of evaporator scales. Proceedings of the 12th conference of the Australian Society of Sugar Cane Technologists (ASSCT), Townsville, Queensland, Australia, Watson Ferguson and Company, Queensland, Australia.

Jones, W. P. and B. E. Launder (1972). "The prediction of laminarisation with a two-equation model of turbulence." International Journal of Heat and Mass Transfer(15): 301-314.

Lance, M. and J. Bataille (1991). "Turbulence in the liquid phase of a uniform bubbly air-water flow." Journal of Fluid Mechanics(222): 95-118.

Lehnberger, A. (1996). "Tubular and plate evaporators for sugar factories." Zuckerindustrie **Vol 121**(No 46): 791 - 798.

Liovic, P., D. Lakehal, et al. (2003). "LES of Turbulent Bubble Formation and Break-up using Interface Tracking-based Simulation." Direct and Large Eddy Simulation-5, Technical University of Munich, Garching, Germany(27-29 August): 8pp.

Peacock, S. D. (1999). A survey of the literature regarding Robert evaporators. Durban, South Africa, Sugar Milling Research Institute (SMRI): 85.

Pennisi, S. (2002). Summary of evaporator test results - Proserpine Mill, #4 evaporator, 2002 crushing season. Mackay, Queensland, Australia, Sugar Research Institute (SRI): 54.

Queensland Sugar Corporation (2001). Sugar Notes. Brisbane, Australia, Queensland Sugar Corporation Limited.

Quinan, P. B., P. J. Degnian, et al. (1985). Design, construction and performance of a large evaporator vessel at Fairymead Mill. Proceedings of the 7th conference of the Australian Society of Sugar Cane Technologists (ASSCT), Bundaberg, Queensland, Australia, Watson Ferguson and Company, Queensland, Australia.

Rohsenow, W. M. (1952). "A method of correlating heat transfer data for surface boiling liquids." ASME **74**: 969.

Rural Press Qld (1998). Australian Sugar Year Book. Ormiston, Australia, Rural Press (Qld) Pty Ltd.

Rural Press Qld (2001). Australian Sugar Year Book. Ormiston, Australia, Rural Press (Qld) Pty Ltd.

Steindl, R. J. and G. D. Ingram (1999). Improved evaporator performance through circulation modelling. Mackay, Queensland, Australia, Sugar Research Institute (SRI): 44.

Stephens, D. W. (2001). Modelling natural circulation in batch vacuum pans. Mechanical Engineering. Townsville, Australia, James Cook University: 267.

Tromp, L. A. (1966). "Tube spacing in heating apparatus, parts I and II." International Sugar Journal **Vol 68**: 163 - 165.

Watson, L. J. (1986). Heat transfer performance in evaporators Part 1 theory and mechanisms. Mackay, Queensland, Australia, Sugar Research Institute (SRI): 56.

Watson, L. J. (1986a). Performance of the new Fairymead evaporator. Proceedings of the 8th conference of the Australian Society of Sugar Cane Technologists (ASSCT), Townsville, Queensland, Australia, Watson Ferguson and Company, Queensland, Australia.

Watson, L. J. (1987). Heat transfer mechanisms in evaporators. Proceedings of the 9th conference of the Australian Society of Sugar Cane Technologists (ASSCT), Mackay, Queensland, Australia, Watson Ferguson and Company, Queensland, Australia.

Wright, P. G. (1983). Juice heating and evaporation processes in the cane raw sugar industry. Proceedings of the 11th Chemical Engineering Conference (CHEMICA), Brisbane, Queensland, Australia, EA Books St Leonards, New South Wales, Australia.

Wright, P. G. (1988). Entrainment separation devices in raw sugar processing. Proceedings of the 10th conference of the Australian Society of Sugar Cane Technologists (ASSCT), Cairns, Queensland, Australia, Watson Ferguson and Company, Queensland, Australia.

Wright, P. G. (2000). Sugar factory configurations for increased cogeneration. Proceedings of the 22nd conference of the Australian Society of Sugar Cane Technologists (ASSCT), Bundaberg, Queensland, Australia, Watson Ferguson and Company, Queensland, Australia.

Appendix A – Glossary of terms

Brix: Is the concentration (in g solute per 100 g solution) of a solution of pure sucrose in water, having the same density as the solution at the same temperature. If refractive index were adopted as an alternative basis of comparison the value derived should be termed refractometer brix.

Calandria: Is the term used to describe the heating element in tubular type evaporators and vacuum pans. A calandria is a series of vertical heating tubes held between two horizontal tube-plates with boiling liquid inside the tubes and condensing LP steam or vapour on the outside.

Dry mass (or dry substance): Is the weight of material remaining after drying the product examined under specified conditions, expressed as a percentage of the original weight. The determination of dry substance represents an attempt to measure the total solids, both soluble and insoluble, or, in the absence of insoluble solids, the total soluble solids. The degree of accuracy achieved depends upon the constitution of the sample and the drying technique.

Effect: Is a term sometimes used to describe one stage of the evaporator station. eg. The #2 effect is the second vessel in the set.

Evaporator Supply Juice (ESJ): Is the term given to the juice after it has been through the clarification and heating stages and is about to enter the evaporator station.

Headspace: Is that part of an evaporator vessel above the calandria where the vapour released from the boiling liquid is contained.

Impurities (soluble): Is a collective term for all substances other than sucrose present in the total soluble solids contained in a sample; sometimes expressed as a percentage of the whole material, and sometimes as a percentage of the total soluble solids.

Juice: Is the term given to the liquid containing sucrose, impurities and water, that is squeezed out of the cane. Usually the material holds the term juice through the various stages of processing until it leaves the final effect of the evaporator station when it is called either syrup or liquor.

Liquor: Is the concentrated sugar solution leaving the final evaporation stage. Sometime also called syrup.

Low pressure (LP) steam: Is that steam which is discharged from turbo machinery such as mills and alternator drives. The steam contains minimal superheat at slightly higher than atmospheric pressures and is unsuitable for driving turbines. However, it still contains a large amount of latent heat energy suitable for heating duties elsewhere in the factory.

Appendix A – Glossary of terms

Massecuite: Is a mixture of sugar crystals and mother molasses liquor discharged from a vacuum pan.

Molasses: Is the mother liquid separated from the massecuite by centrifugal screens.

Pan or Vacuum pan: Is a vessel used to grow sugar crystals in the massecuite by boiling under high vacuum.

Purity: Is the percentage of sucrose contained within the total solids of the solution.

$$Purity = \frac{sucrose\_mass}{dry\_mass}$$

Strike: Is the term given to each cycle of a batch vacuum pan.

Sugar: Is the name given to the crystals of sucrose, together with any adhering molasses, as recovered from the massecuites. The various grades of sugar found in a raw sugar factory are identified in terms of the grade of massecuite they originated from, or in terms of the avenue of disposal. eg. 'A' sugar, 'B' sugar, 'C' sugar, or 'Shipment' sugar.

Syrup: The concentrated sugar solution leaving the final evaporation stage. Sometime also called liquor.

Thermal energy model: The thermal energy model predicts the transport of enthalpy through the fluid domain. It differs from the total energy model in that the effect of mean flow kinetic energy is not included.

Total energy model: The total energy model includes the thermal energy model equations as well as the kinetic energy terms in the equation. This model is suitable for compressible flows where significant changes in density occur.

Appendix B – Example heat & mass balance calculations

Following is an example of the heat and mass balance calculations performed on the Proserpine #4 vessel for test number 1.

Values taken from Table 3.3 are detailed as follows:

Juice flow rate at inlet:	258.2 $m^3 \cdot h^{-1}$
Calandria pressure:	62.3 kPa abs
Headspace pressure:	13.7 kPa abs
Condensate flow rate:	136.3 $m^3 \cdot h^{-1}$
Juice brix at inlet:	35.6%
Juice brix at outlet:	63.1%
Juice temperature at inlet (before flash)	87.8°C

Fluid properties taken from steam tables are as follows:

Calandria saturated vapour temperature	= saturation temperature at calandria pressure = 86.9°C
Headspace saturated vapour temperature	= saturation temperature at headspace pressure = 52.2°C
Enthalpy of vapour	= enthalpy of saturated vapour at headspace pressure = 2595 $kJ \cdot kg^{-1}$
Latent heat of evaporation	= Latent heat of saturated vapour at headspace pressure = 2377 $kJ \cdot kg^{-1}$
Latent heat of condensation	= Latent heat of saturated vapour at calandria pressure = 2289 $kJ \cdot kg^{-1}$
Density of condensate	= Density of saturated vapour at calandria pressure = 9670 $kg \cdot m^{-3}$

Boiling point elevations calculated using equation D-4 as follows:

Boiling point elevation at inlet	= 0.86°C
Boiling point elevation at outlet	= 3.04°C

Juice density at inlet calculated using equation D-1 as follows:

Specific heat of juice calculated using equation D-5 as follows:

Specific heat of juice at inlet	= 3.54 kJ·kg^{-1}·K^{-1}
Juice density at inlet	= 1122 kg·m^{-3}
Mass flow rate of condensate ($\dot{m}_c$)	= Condensate flow rate x Density of condensate = (136.3 m^3·h^{-1} x 9670 kg·m^{-3}) / 1000 = 131.9 t·h^{-1}

Estimated juice temperature at inlet (after flash)

	= Headspace saturated vapour temperature + Boiling point elevation at inlet = 52.2°C + 0.86°C = 53.1°C
Estimated juice temperature at outlet	= Headspace saturated vapour temperature + Boiling point elevation at outlet = 52.2°C + 3.04°C = 55.2°C
Mass flow rate of juice at inlet	= Flow rate of juice at inlet x Density of juice at inlet = (258.2 m^3·h^{-1} x 1122 kg·m^{-3}) / 1000 = 289.8 t·h^{-1}
Mass flow rate of water removed	= Mass flow rate of juice at inlet – (Mass flow rate of juice x (Juice brix at inlet / Juice brix at outlet)) = 289.8 t·h^{-1} - (289.8 t·h^{-1} x (35.6% / 63.1%)) = 126.2 t·h^{-1}
Mass flow rate of juice at outlet	= Mass flow rate of juice at inlet – Mass flow rate of water removed = 289.8 t·h^{-1}-126.2 t·h^{-1} = 163.6 t·h^{-1}
Enthalpy of juice at inlet	= Specific heat of juice at inlet x Juice temperature at inlet (before flash) = 3.54 kJ·kg^{-1}·K^{-1} x 87.8°C = 311 kJ·kg^{-1}

Enthalpy of juice after flashing = Specific heat of juice at inlet x Estimated juice temperature at inlet (after flash)
= 3.54 kJ·kg^{-1}·K^{-1} x 53.1°C
= 188 kJ·kg^{-1}

Vapour fraction after flashing = (Enthalpy of juice at inlet - Enthalpy of juice after flashing) / (Enthalpy of vapour - Enthalpy of juice after flashing)
= (311 kJ·kg^{-1} - 188 kJ·kg^{-1}) / (2595 kJ·kg^{-1} - 188 kJ·kg^{-1})
= 0.051

Mass flow rate of vapour due to flashing = Mass flow rate of juice at inlet x Vapour fraction after flashing
= 289.8 t·h^{-1} x 0.051
= 14.8 t·h^{-1}

Mass flow rate of water evaporated by calandria (m_e)
= Mass flow rate of water removed - Mass flow rate of vapour due to flashing
= 126.2 t·h^{-1} - 14.8 t·h^{-1}
= 111.4 t·h^{-1}

Heat required for evaporation (Q_e) calculated using equation 3.1 as follows:
= 2377 kJ·kg^{-1} x 111.4 t·h^{-1} x (1 / 3600)
= 73.52 MW

Heat required for condensation (Q_c) calculated using equation 3.2 as follows:
= 2289 kJ·kg^{-1} x 131.9 t·h^{-1} x (1 / 3600)
= 83.90 MW

Appendix C – CFX Input File

Following is a copy of the CFX Input File used to model the Proserpine #4 vessel with boundary conditions described by test #1. The Input File contains details of all of the standard features within CFX that were used and all of the user defined sub-routines added to the model.

```
Installed patches:

 * CFX-Build 5 Patch 200307111335

 * CFX-Post Patch 200307041717

 * CFX-Pre Patch 200307091811

 * CFX-5 SolverManager Patch 200306300826
 * CFX-5.6 Solver Patch 200306300826

Setting up CFX-5 Solver run ...


+--------------------------------------------------------------------+
|                                                                    |
|                    CFX Command Language for Run                    |
|                                                                    |
+--------------------------------------------------------------------+

LIBRARY :
  CEL :
    FUNCTION : ramp
      Argument List = []
      Option = Interpolation
      Result Units = []
      INTERPOLATION DATA :
        Data Pairs = 0, 0, \
                     50, 1, \
                     5000, 1
        Extend Max = No
        Extend Min = No
      END
    END
    EXPRESSIONS :
      BPET = 6.064E-05[K^-0.62]*((T^2*(brix*100[])^2)/((647.45[K]-
T)^0.38))\
 *(5.84E-07[]*(((brix*100[])-40[])^2)+7.2E-04[])
      Csf = 0.013[]
      open area ratio = 0.921[]
      saturation temperature = 52.2[C]
      vapour density = 9.2E-02[kg m^-3]
      calandria height = 1.981[m]
      boiling = step((T-(saturation temperature+BPET-
0.001[K]))/1[K])*step(\
 (calandria height-y)/1[m])*step(y/1[m])
```

```
        calandria CSA = 67.3[m^2]-1.044[m^2]
        calandria volume = 133.4[m^3]-2.068[m^3]
        liquid surface tension = 0.071[N m^-1]
        calandria HSA = 5265.7[m^2]
        liquid specific heat = 3.16[kJ kg^-1 K^-1]
        liquid thermal conductivity = 0.574[W m^-1 K^-1]+1.699E-03[W m^-1
K^-\
 2]*(T-273.15[K])-3.608E-06[W m^-1 K^-3]*(T-273.15[K])^2-3.528E-03[W m^-1
K^\
 -1]*(brix*100[])
        liquid viscosity = 4.3E-04[Pa s]*e^(3.357[]*((brix*100[])-
0.3155[K^-1\
 ]*(T-273.15[K]))/(116.8[]-((brix*100[])-0.3155[K^-1]*(T-323.15[K]))))
        Pr = liquid specific heat*liquid viscosity/liquid thermal
conductivit\
 y
        n = 1.0[]
        effective delta T = 31.7[K]
        latent heat = 2377[kJ kg^-1]
        Ja = liquid specific heat*effective delta T/latent heat
        gravity = 9.81[m s^-2]
        liquid density = 1005.3[kg m^-3]-0.22556[kg m^-3 K^-1]*saturation
tem\
 perature-2.4304E-03[kg m^-3 K^-2]*saturation temperature^2+3.7329[kg m^-
3]*\
 (brix*100[])+0.01781937[kg m^-3]*(brix*100[])^2
        qcalc = liquid viscosity*latent heat*((gravity*(liquid density-
vapou\
 r density))/liquid surface tension)^0.5*(Ja/(Pr^n*Csf))^3
        heating on = 1.0[]
        qflow = qcalc*calandria HSA*heating on
        mdot = qflow/latent heat
        evaporation = (mdot/calandria volume)*boiling
        froth quality = 0.0[]
        average vapour velocity = (evaporation*calandria volume)/(vapour
dens\
 ity*calandria CSA*open area ratio)+1.0E-05[m s^-1]
        fluid quality = (vapour density*average vapour velocity/(liquid
densi\
 ty*abs(v)+vapour density*average vapour velocity))*boiling+(step((y-
calandr\
 ia height)/1[m])*froth quality)
        Eulerian density = (fluid quality/vapour density+(1[]-fluid
quality)/\
 liquid density)^-1
        Eulerian velocity = (fluid quality/average vapour velocity+(1[]-
flui\
 d quality)/(abs(v)+1.0E-05[m s^-1]))^-1
        vapour viscosity = 1.1E-05[Pa s]
        Eulerian viscosity = (fluid quality/vapour viscosity+(1[]-fluid
quali\
 ty)/liquid viscosity)^-1
        heating tube ID = 0.042[m]
        Re = ((Eulerian density*Eulerian velocity*heating tube
ID)/Eulerian v\
 iscosity)
        dtake ID = 0.154[m]
        Re2 = ((liquid density*abs(v)*dtake ID)/liquid viscosity)
        boil temperature = saturation temperature+BPET
        buoyancy = -gravity*(Eulerian density-1000.0[kg m^-3])
```

```
      buoyancy2 = -gravity*(liquid density-1000.0[kg m^-3])
      coeff01 = ramp(aitern)
      diffusivity = 7.7E-06[m^2 s^-1]
      ff = 0.027[]+53.333[]/Re
      ff2 = 0.027[]+53.333[]/Re2
      frictionu = -50.0[m^-1]*density*sqrt(u^2+v^2+w^2)*u
      frictionuu = -50.0[m^-1]*density*sqrt(u^2+v^2+w^2)
      frictionv = -ff*((abs(v)/open area ratio)^2*Eulerian
density/2[]*heat\
 ing tube ID*1.0[m^-2])
      frictionvv = -ff2*((abs(v)/open area ratio)^2*liquid
density/2[]*dtak\
 e ID*1.0[m^-2])
      frictionw = -50.0[m^-1]*density*sqrt(u^2+v^2+w^2)*w
      inlet flow rate = 80.5[kg s^-1]
      heat = ((inlet flow rate*liquid specific heat*BPET)/calandria
volume)\
 *heating on
      inlet brix = 0.356[]
      inlet temperature = 53.1[C]
      monitorvalue = massFlowAve(brix)@outlet
      number of segments = 4[]
    END
  END
  ADDITIONAL VARIABLE : brix
    Option = Definition
    Units = [ kg kg^-1 ]
    Variable Type = Specific
  END
  ADDITIONAL VARIABLE : quality
    Option = Definition
    Units = [  ]
    Variable Type = Unspecified
  END
  ADDITIONAL VARIABLE : boiling temperature
    Option = Definition
    Units = [ C ]
    Variable Type = Unspecified
  END
  ADDITIONAL VARIABLE : Reynolds number
    Option = Definition
    Units = [  ]
    Variable Type = Unspecified
  END
  ADDITIONAL VARIABLE : mean density
    Option = Definition
    Units = [ kg m^-3 ]
    Variable Type = Unspecified
  END
  ADDITIONAL VARIABLE : vapour velocity
    Option = Definition
    Units = [ m s^-1 ]
    Variable Type = Unspecified
  END
  MATERIAL : juice
    Option = Pure Substance
    Thermodynamic State = Liquid
    PROPERTIES :
      Absorption Coefficient = 1 [m^-1]
      Density = liquid density
```

```
      Dynamic Viscosity = liquid viscosity
      Molar Mass = 18.02 [kg kmol^-1]
      Option = General Fluid
      Reference Pressure = 101325 [Pa]
      Reference Temperature = 100 [C]
      Refractive Index = 0
      Scattering Coefficient = 0 [m^-1]
      Specific Heat Capacity = liquid specific heat
      Thermal Conductivity = liquid thermal conductivity
    END
  END
END
EXECUTION CONTROL :
  PARALLEL HOST LIBRARY :
    HOST DEFINITION : palms
      Number of Processors = 1
      Installation Root = /usr/local/cfx/5.6
      Host Architecture String = intel_p4.sse_linux2.2.5
    END
    HOST DEFINITION : nebia.sri.org.au
      Host Architecture String = intel_p4.sse_linux2.2.5
    END
  END
  PARTITIONER STEP CONTROL :
    Runtime Priority = Standard
    MEMORY CONTROL :
      Memory Allocation Factor = 1
    END
    PARTITIONING TYPE :
      MeTiS Type = k-way
      Option = MeTiS
      Partition Size Rule = Automatic
      Partition Weight Factors = 0.500, 0.500
    END
  END
  RUN DEFINITION :
    Definition File =
/data/steve/2887/04_Pros/08_cfx5.6/07/run_01/Proserpi\
ne4.def
    Run Mode = Full
  END
  SOLVER STEP CONTROL :
    Runtime Priority = Standard
    EXECUTABLE SELECTION :
      Double Precision = Off
      Use 64 Bit = Off
    END
    MEMORY CONTROL :
      Memory Allocation Factor = 1
    END
    PARALLEL ENVIRONMENT :
      Option = Distributed Parallel
      Parallel Host List = nebia.sri.org.au,palms
      Parallel Mode = PVM
    END
  END
END
FLOW :
  SOLUTION UNITS :
    Angle Units = [rad]
```

Appendix C – CFX Input File

```
  Length Units = [m]
  Mass Units = [kg]
  Solid Angle Units = [sr]
  Temperature Units = [K]
  Time Units = [s]
END
SIMULATION TYPE :
  Option = Steady State
END
SOLVER CONTROL :
  CONVERGENCE CONTROL :
    Maximum Number of Iterations = 500
    Physical Timescale = 1 [s]
    Timescale Control = Physical Timescale
  END
  CONVERGENCE CRITERIA :
    Conservation Target = 0.01
    Residual Target = 1.E-4
    Residual Type = RMS
  END
  ADVECTION SCHEME :
    Option = High Resolution
  END
  DYNAMIC MODEL CONTROL :
    Global Dynamic Model Control = Yes
  END
  EQUATION CLASS : av
    ADVECTION SCHEME :
      Option = High Resolution
    END
    CONVERGENCE CONTROL :
      Physical Timescale = 60 [s]
      Timescale Control = Physical Timescale
    END
  END
  EQUATION CLASS : energy
    ADVECTION SCHEME :
      Option = High Resolution
    END
    CONVERGENCE CONTROL :
      Physical Timescale = 60 [s]
      Timescale Control = Physical Timescale
    END
  END
END
DOMAIN : wholedomain
  Coord Frame = Coord 0
  Domain Type = Fluid
  Fluids List = juice
  Location = Assembly 1
  DOMAIN MODELS :
    BUOYANCY MODEL :
      Option = Non Buoyant
    END
    DOMAIN MOTION :
      Option = Stationary
    END
    REFERENCE PRESSURE :
      Reference Pressure = 0 [Pa]
    END
```

```
END
FLUID MODELS :
  ADDITIONAL VARIABLE : Reynolds number
    Additional Variable Value = Re
    Option = Algebraic Equation
  END
  ADDITIONAL VARIABLE : boiling temperature
    Additional Variable Value = boil temperature
    Option = Algebraic Equation
  END
  ADDITIONAL VARIABLE : brix
    Kinematic Diffusivity = diffusivity
    Option = Transport Equation
  END
  ADDITIONAL VARIABLE : mean density
    Additional Variable Value = Eulerian density
    Option = Algebraic Equation
  END
  ADDITIONAL VARIABLE : quality
    Additional Variable Value = fluid quality
    Option = Algebraic Equation
  END
  ADDITIONAL VARIABLE : vapour velocity
    Additional Variable Value = average vapour velocity
    Option = Algebraic Equation
  END
  HEAT TRANSFER MODEL :
    Option = Thermal Energy
  END
  TURBULENCE MODEL :
    Option = k epsilon
  END
  TURBULENT WALL FUNCTIONS :
    Option = Scalable
  END
END
INITIALISATION :
  Coord Frame = Coord 0
  Frame Type = Stationary
  Option = Automatic
  INITIAL CONDITIONS :
    Velocity Type = Cartesian
    ADDITIONAL VARIABLE : brix
      Additional Variable Value = inlet brix
      Option = Automatic with Value
    END
    CARTESIAN VELOCITY COMPONENTS :
      Option = Automatic
    END
    EPSILON :
      Option = Automatic
    END
    K :
      Option = Automatic
    END
    STATIC PRESSURE :
      Option = Automatic
    END
    TEMPERATURE :
      Option = Automatic with Value
```

```
        Temperature = inlet temperature
      END
    END
  END
  BOUNDARY : wholedomain Default
    Boundary Type = WALL
    Location = BOTTOMSIDES,FROTHSIDES,INLETPIPE,OUTLETPIPE,SYMPLANE1
3,SY\
 MPLANE1 4,SYMPLANE1 5,SYMPLANE1 6
    BOUNDARY CONDITIONS :
      WALL ROUGHNESS :
        Option = Smooth Wall
      END
      WALL INFLUENCE ON FLOW :
        Option = No Slip
      END
      HEAT TRANSFER :
        Option = Adiabatic
      END
      ADDITIONAL VARIABLE : brix
        Option = Zero Flux
      END
    END
  END
  SUBDOMAIN : juicedomain
    Coord Frame = Coord 0
    Location = JUICE DOMAIN
    SOURCES :
      MOMENTUM SOURCE :
        GENERAL MOMENTUM SOURCE :
          Momentum Source X Component = 0.0 [kg m^-2 s^-2]
          Momentum Source Y Component = buoyancy2
          Momentum Source Z Component = 0.0 [kg m^-2 s^-2]
        END
      END
    END
  END
  SUBDOMAIN : calandria
    Coord Frame = Coord 0
    Location = CALANDRIA
    SOURCES :
      EQUATION SOURCE : brix
        Option = Source
        Source = evaporation*brix
      END
      EQUATION SOURCE : continuity
        Option = Fluid Mass Source
        Source = -evaporation
        VARIABLE : T
          Option = Value
          Value = 0.0 [K]
        END
        VARIABLE : brix
          Option = Value
          Value = 0.0 [m m^-1]
        END
        VARIABLE : ed
          Option = Value
          Value = 0.0 [m^2 s^-3]
        END
```

```
        VARIABLE : ke
          Option = Value
          Value = 0.0 [m^2 s^-2]
        END
        VARIABLE : vel
          Option = Cartesian Vector Components
          xValue = 0.0 [m s^-1]
          yValue = 0.0 [m s^-1]
          zValue = 0.0 [m s^-1]
        END
      END
      EQUATION SOURCE : energy
        Option = Source
        Source = heat
      END
      MOMENTUM SOURCE :
        GENERAL MOMENTUM SOURCE :
          Momentum Source Coefficient = frictionuu
          Momentum Source X Component = frictionu
          Momentum Source Y Component = buoyancy+frictionv
          Momentum Source Z Component = frictionw
        END
      END
    END
  END
  BOUNDARY : outlet
    Boundary Type = OUTLET
    Location = OUTLET
    BOUNDARY CONDITIONS :
      FLOW REGIME :
        Option = Subsonic
      END
      MASS AND MOMENTUM :
        Option = Static Pressure
        Relative Pressure = 0.0 [Pa]
      END
    END
  END
  BOUNDARY : symm1
    Boundary Type = SYMMETRY
    Location = SYMPLANE1
  END
  BOUNDARY : symm2
    Boundary Type = SYMMETRY
    Location = SYMPLANE2
  END
  BOUNDARY : top surface
    Boundary Type = WALL
    Location = TOPSURFACE
    BOUNDARY CONDITIONS :

      ADDITIONAL VARIABLE : brix
        Option = Zero Flux
      END
      HEAT TRANSFER :
        Option = Adiabatic
      END
      WALL INFLUENCE ON FLOW :
        Option = Free Slip
      END
```

```
    END
  END
  BOUNDARY : deflector
    Boundary Type = WALL
    Location = DEFLECTOR
    BOUNDARY CONDITIONS :
      ADDITIONAL VARIABLE : brix
        Option = Zero Flux
      END
      HEAT TRANSFER :
        Option = Adiabatic
      END
      WALL INFLUENCE ON FLOW :
        Option = No Slip
      END
      WALL ROUGHNESS :
        Option = Smooth Wall
      END
    END
  END
  BOUNDARY : inlet
    Boundary Type = INLET
    Location = INLET
    BOUNDARY CONDITIONS :
      ADDITIONAL VARIABLE : brix
        Additional Variable Value = inlet brix
        Option = Value
      END
      FLOW DIRECTION :
        Option = Normal to Boundary Condition
      END
      FLOW REGIME :
        Option = Subsonic
      END
      HEAT TRANSFER :
        Option = Static Temperature
        Static Temperature = inlet temperature
      END
      MASS AND MOMENTUM :
        Mass Flow Rate = inlet flow rate/number of segments
        Option = Mass Flow Rate
      END
      TURBULENCE :
        Option = Medium Intensity and Eddy Viscosity Ratio
      END
    END
  END
  SUBDOMAIN : froth
    Coord Frame = Coord 0
    Location = FROTH DOMAIN
    SOURCES :
      MOMENTUM SOURCE :
        GENERAL MOMENTUM SOURCE :
          Momentum Source X Component = 0.0 [kg m^-2 s^-2]
          Momentum Source Y Component = buoyancy
          Momentum Source Z Component = 0.0 [kg m^-2 s^-2]
        END
      END
    END
  END
```

```
BOUNDARY : calandria walls
  Boundary Type = WALL
  Location = CALWALLSINT
  BOUNDARY CONDITIONS :
    ADDITIONAL VARIABLE : brix
      Option = Zero Flux
    END
    HEAT TRANSFER :
      Option = Adiabatic
    END
    WALL INFLUENCE ON FLOW :
      Option = Free Slip
    END
  END
END
BOUNDARY : calandria walls ext
  Boundary Type = WALL
  Location = CALWALLSEXT
  BOUNDARY CONDITIONS :
    ADDITIONAL VARIABLE : brix
      Option = Zero Flux
    END
    HEAT TRANSFER :
      Option = Adiabatic
    END
    WALL INFLUENCE ON FLOW :
      Option = Free Slip
    END
  END
END
BOUNDARY : dtake walls
  Boundary Type = WALL
  Location = DTAKEWALLS
  BOUNDARY CONDITIONS :
    ADDITIONAL VARIABLE : brix
      Option = Zero Flux
    END
    HEAT TRANSFER :
      Option = Adiabatic
    END
    WALL INFLUENCE ON FLOW :
      Option = Free Slip
    END
  END
END
SUBDOMAIN : dtake 1A
  Coord Frame = Coord 0
  Location = DTAKE1A
  SOURCES :
    MOMENTUM SOURCE :
      GENERAL MOMENTUM SOURCE :
        Momentum Source X Component = 0.0 [kg m^-2 s^-2]
        Momentum Source Y Component = buoyancy2+frictionvv
        Momentum Source Z Component = 0.0 [kg m^-2 s^-2]
      END
    END
  END
END
SUBDOMAIN : dtake 1B
  Coord Frame = Coord 0
```

```
    Location = DTAKE1B
    SOURCES :
      MOMENTUM SOURCE :
        GENERAL MOMENTUM SOURCE :
          Momentum Source X Component = 0.0 [kg m^-2 s^-2]
          Momentum Source Y Component = buoyancy2+frictionvv
          Momentum Source Z Component = 0.0 [kg m^-2 s^-2]
        END

      END
    END
  END
  SUBDOMAIN : dtake 1C
    Coord Frame = Coord 0
    Location = DTAKE1C
    SOURCES :
      MOMENTUM SOURCE :
        GENERAL MOMENTUM SOURCE :
          Momentum Source X Component = 0.0 [kg m^-2 s^-2]
          Momentum Source Y Component = buoyancy2+frictionvv
          Momentum Source Z Component = 0.0 [kg m^-2 s^-2]
        END
      END
    END
  END
  SUBDOMAIN : dtake 1D
    Coord Frame = Coord 0
    Location = DTAKE1D
    SOURCES :
      MOMENTUM SOURCE :
        GENERAL MOMENTUM SOURCE :
          Momentum Source X Component = 0.0 [kg m^-2 s^-2]
          Momentum Source Y Component = buoyancy2+frictionvv
          Momentum Source Z Component = 0.0 [kg m^-2 s^-2]
        END
      END
    END
  END
  SUBDOMAIN : dtake 1E
    Coord Frame = Coord 0
    Location = DTAKE1E
    SOURCES :
      MOMENTUM SOURCE :
        GENERAL MOMENTUM SOURCE :
          Momentum Source X Component = 0.0 [kg m^-2 s^-2]
          Momentum Source Y Component = buoyancy2+frictionvv
          Momentum Source Z Component = 0.0 [kg m^-2 s^-2]
        END
      END
    END
  END
  SUBDOMAIN : dtake 2A
    Coord Frame = Coord 0
    Location = DTAKE2A
    SOURCES :
      MOMENTUM SOURCE :
        GENERAL MOMENTUM SOURCE :
          Momentum Source X Component = 0.0 [kg m^-2 s^-2]
          Momentum Source Y Component = buoyancy2+frictionvv
          Momentum Source Z Component = 0.0 [kg m^-2 s^-2]
```

```
        END
      END
    END
  END
  SUBDOMAIN : dtake 2B
    Coord Frame = Coord 0
    Location = DTAKE2B
    SOURCES :
      MOMENTUM SOURCE :
        GENERAL MOMENTUM SOURCE :
          Momentum Source X Component = 0.0 [kg m^-2 s^-2]
          Momentum Source Y Component = buoyancy2+frictionvv
          Momentum Source Z Component = 0.0 [kg m^-2 s^-2]
        END
      END
    END
  END
  SUBDOMAIN : dtake 2C
    Coord Frame = Coord 0
    Location = DTAKE2C
    SOURCES :
      MOMENTUM SOURCE :
        GENERAL MOMENTUM SOURCE :
          Momentum Source X Component = 0.0 [kg m^-2 s^-2]
          Momentum Source Y Component = buoyancy2+frictionvv
          Momentum Source Z Component = 0.0 [kg m^-2 s^-2]
        END
      END
    END
  END
  SUBDOMAIN : dtake 2D
    Coord Frame = Coord 0
    Location = DTAKE2D
    SOURCES :
      MOMENTUM SOURCE :
        GENERAL MOMENTUM SOURCE :
          Momentum Source X Component = 0.0 [kg m^-2 s^-2]
          Momentum Source Y Component = buoyancy2+frictionvv
          Momentum Source Z Component = 0.0 [kg m^-2 s^-2]
        END
      END
    END
  END
  SUBDOMAIN : dtake 2E
    Coord Frame = Coord 0
    Location = DTAKE2E
    SOURCES :
      MOMENTUM SOURCE :
        GENERAL MOMENTUM SOURCE :
          Momentum Source X Component = 0.0 [kg m^-2 s^-2]
          Momentum Source Y Component = buoyancy2+frictionvv
          Momentum Source Z Component = 0.0 [kg m^-2 s^-2]
        END
      END
    END
  END
  SUBDOMAIN : dtake 3A
    Coord Frame = Coord 0
    Location = DTAKE3A
    SOURCES :
```

```
      MOMENTUM SOURCE :
        GENERAL MOMENTUM SOURCE :
          Momentum Source X Component = 0.0 [kg m^-2 s^-2]
          Momentum Source Y Component = buoyancy2+frictionvv
          Momentum Source Z Component = 0.0 [kg m^-2 s^-2]
        END
      END
    END
  END
  SUBDOMAIN : dtake 3B
    Coord Frame = Coord 0
    Location = DTAKE3B
    SOURCES :
      MOMENTUM SOURCE :
        GENERAL MOMENTUM SOURCE :
          Momentum Source X Component = 0.0 [kg m^-2 s^-2]
          Momentum Source Y Component = buoyancy2+frictionvv
          Momentum Source Z Component = 0.0 [kg m^-2 s^-2]
        END
      END
    END
  END
  SUBDOMAIN : dtake 3C
    Coord Frame = Coord 0
    Location = DTAKE3C
    SOURCES :
      MOMENTUM SOURCE :
        GENERAL MOMENTUM SOURCE :
          Momentum Source X Component = 0.0 [kg m^-2 s^-2]
          Momentum Source Y Component = buoyancy2+frictionvv
          Momentum Source Z Component = 0.0 [kg m^-2 s^-2]
        END
      END
    END
  END
  SUBDOMAIN : dtake 3D
    Coord Frame = Coord 0
    Location = DTAKE3D
    SOURCES :
      MOMENTUM SOURCE :
        GENERAL MOMENTUM SOURCE :
          Momentum Source X Component = 0.0 [kg m^-2 s^-2]
          Momentum Source Y Component = buoyancy2+frictionvv
          Momentum Source Z Component = 0.0 [kg m^-2 s^-2]
        END
      END
    END
  END
  SUBDOMAIN : dtake 4A
    Coord Frame = Coord 0
    Location = DTAKE4A
    SOURCES :
      MOMENTUM SOURCE :
        GENERAL MOMENTUM SOURCE :
          Momentum Source X Component = 0.0 [kg m^-2 s^-2]
          Momentum Source Y Component = buoyancy2+frictionvv
          Momentum Source Z Component = 0.0 [kg m^-2 s^-2]
        END
      END
    END
```

```
    END
    SUBDOMAIN : dtake 4B
      Coord Frame = Coord 0
      Location = DTAKE4B
      SOURCES :
        MOMENTUM SOURCE :
          GENERAL MOMENTUM SOURCE :
            Momentum Source X Component = 0.0 [kg m^-2 s^-2]
            Momentum Source Y Component = buoyancy2+frictionvv
            Momentum Source Z Component = 0.0 [kg m^-2 s^-2]
          END
        END
      END
    END
  END
  OUTPUT CONTROL :
    MONITOR OBJECTS :
      MONITOR POINT : outlet brix
        Expression Value = monitorvalue
        Option = Expression
      END
    END
  END
END
COMMAND FILE :
  Version = 5.6
  Results Version = 5.6
END
```

Appendix D – Fluid property equations

Liquid density, Watson (1986b):

$$\rho_l = 1005.3 - 0.22556T - 2.4304\times10^{-3}T^2 + 3.7329B + 0.01781937B^2 \tag{D-1}$$

Liquid viscosity, Steindl (1981):

$$\mu_l = 4.3\times10^{-4}\exp[3.357(B - 0.3155(T-50))/116.8 - (B - 0.3155(T-50))] \tag{D-2}$$

Liquid thermal conductivity, Watson (1986):

$$\kappa_l = 0.574 + 1.699\times10^{-3}T - 3.608\times10^{-6}T^2 - 3.528\times10^{-3}B \tag{D-3}$$

Boiling point elevation, Peacock (1995):

$$T_e = 6.064\times10^{-5}\left(\frac{(273.15+T)^2B^2}{(374.3-T)^{0.38}}\right)\left(5.84\times10^{-7}(B-40)^2 + 7.2\times10^{-4}\right) \tag{D-4}$$

Enthalpy of liquid, Peacock (1995):

$$Cp_l = 4.125 - 0.024B + 6.7x10^{-5}BT + 1.869x10^{-3}T - 9.271x10^{-6}T^2 \tag{D-5}$$

Appendix E – Proserpine #4 residence time distribution

Table D 1 Tracer test raw data (method detection limit is $4x10^{-5}$ mg/g)

Time (minutes)	Concentration (mg/g)
0.0	0
0.5	0
1.0	0
1.5	0
2.0	0.00073
2.5	0.00044
3.0	
3.5	0.00043
4.0	0.00016
4.5	0.00099
5.0	0.00040
5.5	0.00021
6.0	0.00029
6.5	0.00022
7.0	0.00055
7.5	0.00049
8.0	0.00038
8.5	0.00059
9.0	0.00015
9.5	0
10.0	0.00053
10.5	0
11.0	0
11.5	0.00025
12.0	0.00060
12.5	0
13.0	
13.5	0
14.0	0
14.5	0.00062
15.0	0.00040
15.8	0
16.5	0
17.3	0
18.0	0
18.8	0
19.5	0
20.3	0
21.0	0
21.8	0
22.5	0
23.3	0

Appendix E – Proserpine #4 residence time distribution

24.0	0
24.8	0
25.5	0
26.3	0
27.0	0
27.8	0
28.5	0
29.3	0
30.0	0
31.5	0
33.0	0
34.5	0
36.0	0
37.5	0
39.0	0
40.5	0
42.0	0
43.5	0
45.0	0
48.0	0
51.0	0
54.0	0
57.0	0
60.0	0

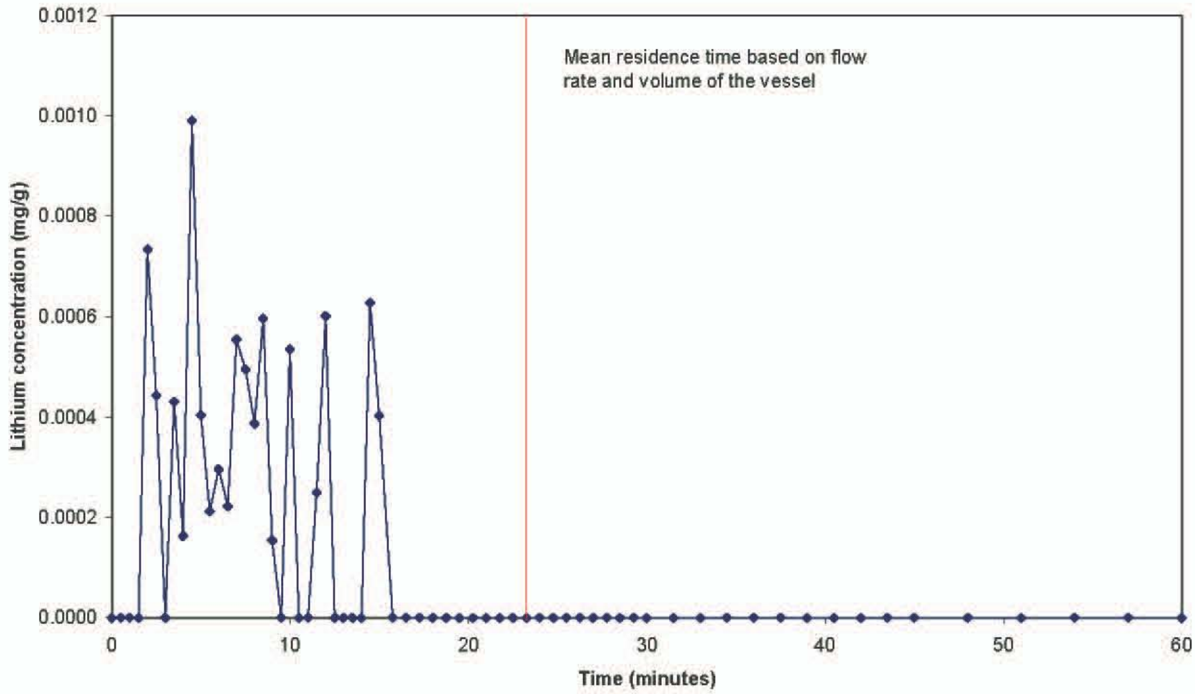

Figure D 1 Residence time distribution plot Proserpine #4